Nanoparticles for Biological and Medical Imaging

Aiguo Wu*

Ningbo Cixi Institute of Biomedical Engineering, Ningbo Institute of Materials Technology and Engineering, Chinese Academy of Sciences, Ningbo 315201, P.R. China

Abstract

Nanotechnology has provided considerable promise for the biological and medical fields, especially in the subjects of biological and medical imaging for the last two decades. Here, we outline different nanoparticles to contribute to biological and medical imaging disciplines. These concerned nanoparticles are soft nanoparticles, which are based on biomacromolecule/polymer or organic molecule components, hard nanoparticles that are derived from various inorganic components and hard-soft nanoparticles that are based on both inorganic components and biomacromolecule/polymer or organic molecule ones. We also discuss the imaging modalities in biology and medicine that various nanoparticles became involved in are: (1) optical imaging (OI), (2) computed tomography (CT), (3) magnetic resonance imaging (MRI), (4) ultrasonography (USG), (5) positron emission tomography (PET). We will also describe various nanoparticles to serve for one/some of those five modalities in biology and medicine imaging in this review paper.

Key Words: nanoparticle, nanomedicine, soft, hard, optical imaging, computed tomography, magnetic resonance imaging, ultrasonography, positron emission tomography.

* An author for correspondence: Tel: +86 (574)86685039; E-mail: aiguo@nimte.ac.cn

CONTENTS

I. Introduction

Nanotechnology is a subject that researches the world of a scale of 1-100 nm in one-, two-, or three-dimension(s). Nanotechnology has provided a broad platform in many disciplines such as biology, medicine, chemistry, physics, materials science, engineering, and more for the last two decades. The focused unit that nanotechnology revolutionizes various scientific fields is embodied in a variety of nanoparticles. In particular nanoparticels make great promise for biology and medicine such as detection, diagnosis, treatment as well as imaging severe diseases for example various tumors/cancers. Here, we want to focus on some work that different nanoparticles offer benefits for biological and medical imaging.

1) Various Nanoparticles for Biological and Medical Imaging

The nanoparticles that are relative to biological and medical imaging include soft nanoparticles, hard nanoparticles, and hard-soft/soft-hard nanoparticles. Their shapes of nanoparticles discussed here may be sphere, rod, tube, needle, cube, cage, and prism so on. Their structures of nanoparticles may be monolayer, core-shell, or multilayer.

(1) Soft Nanoparticles

The soft nanoparticles mentioned in this review will be based on a polymer component, an organic molecule component, or a mixture with both of two components. The polymer includes generally artificial/natural macromolecules and bio-macromolecules for example proteins, peptides, lipids, nucleic acids, and viruses so on. The organic molecules mainly include manmade functional molecules in purpose.

A) Polymer Nanoparticles

The polymer nanoparticles have been produced for several decades for a variety of use in high performance materials and specialty coatings before “nano” became popular. It is easy to form polymer nanoparticles via changing pH value or controlling special interaction ways. The extremely large surface area on the polymer nanoparticles offers many opportunities to put different functional groups on their surfaces. Another benefit that polymer nanoparticles offer is a compatibility with inorganic materials or different types of polymers together. The general used polymer nanoparticles in biological and medical imaging are polymer-drug conjugates, liposomes, micelles, vesicles, dendrimers, nanogels, and nanoshpere (Tong & Cheng, 2007). A third advantage of polymer nanoparticles with good interfacial adhesion eliminates scattering and strengthens an interaction of nanoparticles in the body and increases a retention time in vivo that benefits for applications in biological and medical imaging (Schmidt & Malwitz, 2003; Ekpo MD *et al*., 2022).

B) Organic Nanoparticles

Organic nanoparticles have many forms together with polymer nanoparticels such as pharmaceuticals/ drugs, pigments/dyes, viruses, and protein/nucleic acid aggregates. The properties, in particular the optical and color attributes of organic nanoparticles are controlled by their components, sizes and superamolecular structures. In compare to the hard nanoparticles, it seems a little effect to control their shapes adjusting properties of organic nanoparticles (Horn & Rieger, 2001; Wang *et al.*, 2020).

(2) Hard Nanoparticles

The hard nanoparticles mentioned in this review will be based on an inorganic component, or several types of inorganic ones. The hard nanoparticles mainly include noble metal nanoparticles such as gold

nanoparticles and silver nanoparticles, semiconductor nanoparticles for example the general quantum dots: CdS, ZnS, CdSe, CdTe@ZnS, and other semiconductor nanoparticles such as TiO_2 and SiO_2 and other hard nanoparticles for example SiO_2@Au, FeCo, Gamma-Fe_2O_3, and Fe_3O_4.

A) Metal Nanoparticles

Metal nanoparticles, especially noble metal nanoparticles such as gold and silver have very interesting optical properties because of the known phenomenon of surface plasmon resonance (SPR). This resonance of metal free electrons across the nanoparticles is induced by an electromagnetic filed at a certain frequency while a size of noble metal nanoparticles is much smaller than a wavelength of light. The SPR of the metal electrons causes a strong enhancement absorption and scattering of electromagnetic radiation around the nanoparticles. The SPR of noble metal nanoparticles greatly relies on the composition, size, and shape besides the surrounding media/substrates and inter-particle interactions (Jain, El-Sayed & El-Sayed, 2007; Li *et al.*, 2022).

B) Semiconductor Nanoparticles

The semiconductor nanoparticles refer to their elemental components are from groups II to groups VI in the periodic table. The electronic energy levels in semiconductor nanoparticles are discrete, quantized and the gap of the electronic energy levels can be precisely tuned through variation of their sizes and components. In chemical terms semiconductor nanoparticples are considered inorganic salts or metal oxides (Thurn *et al.*, 2007; Jiang & Tian, 2018).

(a) Quantum Dots

Quantum dots are a specially type of semiconductor nanoparticles that their sizes are down to 10 nm which are smaller than a bulk excitation Bohr radius of the semiconductor materials (Wikipedia, the free encyclopedia: http://en.wikipedia.org/wiki/Quantum_dot). The small size of quantum dots results in their unique photoelectron emission properties. Electrons in the valence band of the quantum dot easily hop to its conductive band after a quantum dot is excited under an external filed. A fluorescent signal will be obtained when those excited electrons with higher energy move back to the valence band along with an emission of photons. Due to this, quantum dots with long fluorescence lifetime (>10 ns) and narrow emission peaks (typically 20-30 nm full width at half maximum) overcome many defects of ‘‘classical’’ organic fluorescent dyes such as photoinstability and wide emission peaks. Moreover, the fluorescence emission wavelengths of quantum dots cover a wide range from UV to near infrared light (NIR, 700-900 nm), which is dependent on their physical size, shape, and chemical components. This is very useful for biological and medical imaging particularly for photoluminescent labels and simultaneous multiple targets (Fu *et al.*, 2005; Thurn *et al.*, 2007; Ornes, 2016)

(b) Titanium Dioxide Nanoparticles

Comparing to the generally used semiconductor nanoparticles such as quantum dots, titanium dioxide nanoparticle (TiO_2) is a wide-gap semiconductor nanoparticle with photocatalytic activity in ultraviolet wavelength (around 380 nm for 4.5 nm of spheric TiO_2 nanoparticles). Upon excitation, TiO_2 nanoparticles can simultaneously trap multiple electrons, producing positively charged holes in the conjugated molecules (if present) or causing formation of oxygen free radicals in the vicinity of the nanoparticle by removal of electrons from the molecules of water in contact with the TiO_2 surface (Thurn *et al.*, 2007). These oxygen free radicals enable oxidation of nearby biomolecules, which may be useful

for therapeutic purposes in future (Thurn *et al.*, 2007). The surface chemistry of TiO_2 nanoparticles smaller than 20 nm depends on formation of "corner defects" on the surface of the nanoparticle, which are very reactive with bidentate ligands such as two-next hydroxyl groups with conjugation structures (Thurn *et al.*, 2007). It offers an easy way to attach or modify the molecules on the surface of TiO_2 nanoparticles (Thurn *et al.*, 2007； Grande & Tucci, 2016).

(c) Other Semiconductor Nanoparticles

Other semiconductor nanoparticles in this review will be silica nanoparticles (SiO_2) and diamond nanoparticles (Nanodiamond). Compared to other semiconductor nanoparticles, silica nanoparticles possess some advantages: (i) SiO_2 nanoparticles are easy to separate, modify on their surface and treating in other solution processes; (ii) SiO_2 nanoparticles are hydrophilic and biocompatible (iii) SiO_2 nanoparticles are no swelling or porosity change with pH changes (Wang & Tan, 2006). It is an ideal candidate for biological and medical imaging (Wang & Tan, 2006). Nanodiamond is highly ordered structures that cell like and soluble in aqueous solutions, which makes them clinically important later (Huang *et al.*, 2007； Wang *et al.*, 2021).

C) Carbon Nanotubes

Carbon nanotubes are a family of tubular nanostructrues reeled from a layer or multiple layers covalently bonded carbon atoms–graphite (Iijima, 1991; Iijima & Ichihashi, 1993; Bethune *et al.*, 1993). The nanotubes that are reeled from one layer of covalently bonded carbon atoms called single-walled nanotubes (SWNTs) and reeled from multiple layers of ones called multiple walled nanotubes (MWNTs). Because of the relatively simple structures and unique properties in physics, mechanics, and electronics

of SWNTs, it is a focus of many researchers. It depends on chiral angle of the formed SWNTs that may be conductive, semiconductive or insulate (Dekker, 1999; Manikandan et al., 2021).

. Semiconductive SWNTs show band gap fluorescent emission in the NIR of between 900 and 1600 nm. It is possible to detect the sharp spectra of SWNTs even in complex biological/medical environments because natural biomolecules are relatively transparent and non-emissive in this region of emission wavelength.

D) Other Hard Nanoparticles

Other hard nanoparticles except noble metal nanoparticles and semiconductor nanoparticles here include some useful nanoparticles with special functions such as FeCo, Gd_2O_3, Fe_3O_4, Gamma-Fe_2O_3 for MRI applications, Bi_2S_3 for CT applications and SiO_2@Au core-shell nanoparticles for optical imaging in near infrared field.

(3) Hard-Soft/Soft-Hard Nanoparticles

The hard-soft or soft-hard nanoparticles mentioned in this review will be based on both inorganic components as a hard layer(s) and polymer or organic molecules as a soft layer(s). The hard layer(s) may be outside or inside of the nanoparticles relying on different application purpose.

2) Different Types of Biological and Medical Imaging

The main types of biological and medical imaging are optical imaging (OI), computed tomography (CT), magnetic resonance imaging (MRI), ultrasoungraphy (USG), and positron emission tomography (PET).

As for the characters, advantages, and disadvantages of these five imaging modalities, they are summarized in Table 1.

(1) Optical imaging (OI)

Optical imaging (OI) is an imaging technique taking advantage of visible or near infrared light, particularly the near infrared light to visualize the objects. It usually includes two kinds of modes: diffusive optical imaging (DOI) or diffuse optical tomography (DOT) (Gibson *et al.*, 2005) and ballistic optical imaging (Farsiu *et al.*, 2007). DOI or DOT is a modality that uses near infrared light to create images of the body. This technique is sensitive to the optical absorption of some compositions in the body. The spatial resolution of DOI or DOT is around several millimeters, which competes with that of a functional magnetic resonance imaging (fMRI) and a temporal resolution of DOI or DOT can reach some milliseconds. The DOI or DOT offers two kinds of information for the objects: i) to detect the absorption of light that is relevant to concentration of chemicals in the body, ii) to detect the scattering of light that is relevant to physiological characteristics for example a swelling of glia or neurons in the brain (Gibson *et al.*, 2005). On the contrary, the ballistic optical imaging ignores the diffusive photons and depends uniquely on the ballistic photons to generate high-resolution images with near diffraction limit of light through scattering media (Farsiu *et al.*, 2007). At this monment, the near-Infrared fluorescent imaging is the widely used techniques in medical and biological fields.

(2) Computed Tomography (CT)

Computed tomography (CT) is medical imaging technique using tomography where a digital geometry processing is employed to create a three-dimensional image of the internals of an object from many of

two-dimensional X-ray images (Wikipedia, the free encyclopedia: en.wikipedia.org/wiki/ Computed_tomography). CT provides a variety of separate anatomical structures based on its capability of blocking an X-ray beam at different depths within the body. The anatomical structures at target level are clear while the other structures at different levels are blurred. Various effects can be obtained by changing the extent and path of motion with a series of depths of field and different degrees of blurring of out-of-plane structures. As a clinically practical imaging method, CT provides some advantages: (i) to exclude the superimposition of images of anatomical structures out-of-plane the area of interest, (ii) to be able to distinguish differences amongst tissues in physical density by less than 1%, (iii) to produce an axial, coronal, or sagittal plane images relying on a specific diagnostic purpose. At the same time CT causes some disadvantages: (i) to be regarded as an ionizing radiation diagnostic technique that can cause some hazards for the patients, (ii) to induce kidney damages to provide superior-quality images intravenously administrating contrast agents for the patients with moderate kidney failure.

Furthermore, there is a special CT method-single photon emission tomography (SPECT) based on a radiation stuff that is administrated at a low mass amount labeled with radioisotopes such as ^{99}mTc (t1/2=6 hours), ^{123}I (t1/2=13.2 hours), ^{131}I (t1/2=8.1 days), and ^{111}In (t1/2=2.8 days) so on. It is distighish from a normal CT method (Wikipedia, the free encyclopedia:en.wikipedia.org/wiki/ Single_photon_ emission_computed_tomography).

(3) Magnetic Resonance Imaging (MRI)

Magnetic resonance imaging (MRI) is a non-invasive way greatly depending on the relaxation properties of proton nuclei in water and lipids to show images of the inside of an object. MRI is widely used in

imaging to show pathological or other physiological changes of living tissues in the body. In comparison with CT, MRI has some advantages: (i) to employ non-ionizing radio frequency (RF) signals to obtain its images and is best matched to non-calcified tissues in the body, (ii) to be able to detect various features in tissues via varying scanning parameters, (iii) to create cross-sectional images in any images besides oblique planes, (iv) to be superior to detect and identify tumors, (v) to be best suited for multiple times examination successively within a short period of time, (vi) to provide multiple contrast mechanisms for example: T1 weighted, T2 weighted, and T2* weighted MR images (Wikipedia, the free encyclopedia: en.wikipedia.org/wiki/Magnetic_resonance_imaging).

In MRI, T1 relaxation also called spin-lattice or longitudinal relaxation that is a time constant of nuclear spins returning to equilibrium. When nuclei are from the high-energy state to the low energy what is related to loss of energy to the surrounding nuclei. T1 relaxation is characterized by the longitudinal return of the net magnetization to its ground state of maximum length along with a direction of the main magnetic field. T1 is usually around 1 second for tissue. T2 relaxation also named spin-spin or transverse relaxation that is a time constant of signal decay. T2 relaxation happens during spins in the high and low energy state exchanging energy but not releasing energy to the surrounding lattice. The magnetic moments interact with each other making a decrease in the transverse magnetization or decay after nuclei release their excess energy. T2 is usually less than 100 ms for general tissue. T2* is a time that occurs for the transverse magnetization to decay to 37% of its original magnitude. It is produced under an inhomogeneous magnetic field and happens in all magnets. It is characterized by inhomogeneous B_0 and loss of transverse magnetization at a rate greater than T2 (Wikipedia, the free encyclopedia: en.wikipedia.org/wiki/Magnetic_resonance_imaging).

(4) Ultrasonography (USG)

Ultrasonography (USG) is an imaging technique based on ultrasound that is a cyclic sound wave with a frequency over the upper limit of human hearing of about 25 kilohertz to visualize muscles, tendons, and other internal organs, their size, structure and any pathological lesions with tomographical images in real time (Wikipedia, the free encyclopedia, http://en.wikipedia.org/wiki/Medical_ultrasonography). A general clinical diagnostic imaging frequency used for ultrasound is 1-10 MHz frequency that shows a sub-millimeter to millimeter (mm) spatial resolution. At higher frequencies, for example 20-50 MHz, ultrasound images provide a higher resolution that is down to tens of micrometers that is suitable for imaging of specific organs, such as in ophthalmology, or in the intravascular probes. At very low frequency for instance, 1-3 MHz, ultrasound images allow deep penetration within the body while at high frequencies ultrasound images only provide a limited penetration, in general several mm (Klibanov, 2005). As a most widely used imaging technique, USG is a relatively cheap and portable tool in contrast to CT or MRI. Up to now USG has been posed no known risks to the patients because of no use of ionizing radiation. There are two potential physiological effects to be caused by ultrasound: (i) to produce microscopic bubbles in living tissues, distort the cell membrane, and influence ion fluxes and intracellular activity, (ii) to generate some small pockets of gas in body fluids or tissues to swell and contract under high intensity of ultrasound.

(5) Positron Emission Tomography (PET)

Positron emission tomography (PET) is an imaging technique with non-invasive, but involving exposure of ionizing radiation that creates a three-dimensional map of functional processes in living subjects at nano- and picomolar levels. It detects gamma rays emitted indirectly by a positron-emitting radioisotope

that enters the body on metabolically active molecules before an image of metabolic activity in space is reconstructed by computer analysis. Usually PET is used in combination with CT to obtain both anatomic and metabolic information in the body. It is very useful in viewing the details of moving organs or structures with higher amounts of anatomical variation (Wikipedia, the free encyclopedia, http://en.wikipedia.org/wiki/Positron_emission_tomography).

II. Nanoparticles for Optical Imaging (OI)

Nanoparticles mainly contributed to optical imaging in biology and medicine are hard nanoparticles such as noble metal nanoparticles, quantum dots (QDs), titanium dioxide nanoparticles, carbon nanotubes, and composite SiO_2 core-Au shell nanoparticles or hard-soft nanoparticles for example peptide-modified QDs, antibody-modified QDs, PEGlated-Au, and oligonucleotide coated silver nanoparticles so on.

1) Metal Nanoparticles and Hard-Soft Nanoparticles Based on Metal

Noble metal nanoparticles such as Au and Ag are superior to the absorbing and fluorescence dyes traditionally used in biological and medical imaging due to a phenomenon of SPR. For instance, Mie theory calculates that an optical cross-section of gold nanoparticles has approximately 4-5 orders of magnification higher than those of organic dyes (Mie, 1908). The SPR-enhanced scattering from gold nanoparticles makes them good promising as optical probes and labels for cancer detections based on imaging. Sokolov and coworkers used immunotargeted gold nanoparticles with a diameter of 12 nm imaging cervical epithelial cancer cells (SiHa cells) known to overexpress the transmembrane glycoprotein, epithelial growth factor receptor (EGFR) (Sokolov, 1999). They employed anti-EGFR

monoclonal antibodies via electrostatic interaction of the antibody molecules to negatively charged surface of gold nanoparticles. The scattering from non-labeling SiHa cells was about 50 folds lower than those of labeled ones. The scattering images of the labeled cells showed that binding of the gold nanoparticle-antibodies occurred mainly on the surface of the cell membranes that confirmed the molecular specific interaction of this labeling technique. El-Sayed *et al.* successfully showed detection and differentiation of cancerous cells from normal cells employing SPR scattering imaging and SPR absorption spectroscopy of 35 nm gold nanoparticles with anti-EGFR antibodies immunotargeted to two epithelial cell lines: human oral squamous carcinomas of HOC 313clone 8 and HSC 3 (El-Sayed *et al.*, 2005). The SPR scattering imaging confirmed the specific binding of the antibodies to EGFR overexpressed on the surface of the cancerous cells and the nanoparticle conjugates accumulating in the cytoplasmic membrane areas. As a control, benign keratinocyte cell lines (HaCaT) incubated with the gold bionanoconjugates show non-specific labeling instead of a random distribution of nanoparticles on the HaCaT cells. Moreover, the strong SPR absorption of gold nanoparticles offers a new way for sensing and quantifying the molecular specific-binding nanoparticle by microabsorption spectroscopy. Both HOC and HSC cells showed a red-shifted by 9 nm after their labeled by gold nanoparticles in solution. The change is a result from the local dielectric environment around the gold nanoparticles because of a binding of the conjugated antibodies with their targets. They also demonstrated that a specific and homogeneous binding of antibody-conjugated gold nanoparticles to the cancer cell surface leads to a sharper SPR absorption peak for cancerous cells in comparison to that of benign cells, where the nanoparticles are bound inhomogenously due to a nonspecific interaction. Also from El-Sayed group, they showed an efficiency of immunotargeted gold nanoparticles as photothermal agents in living cells in vitro in laser microscopy images using the-above-mentioned cell lines. The malignant HOC and HSC

cellular lines suffer photothermal damage within 4 min at laser energy thresholds in contrast to none of the healthy HaCaT cell lines without gold treatment showing any photothermal damage (El-Sayed *et al.*, 2006; Huang *et al.*, 2006a).

The general used gold nanoparticles enable imaging in visible light and can be extended to skin or surface type cancers in vitro, however in vivo imaging applications for deeper tissue require a near-infrared (NIR) region light where tissues have the highest transmissivity (Weissleder, 2001). It depends on a tissue type that the light penetration depth can be up to several centimeters in spectral region 700-900 nm that is known as biological NIR window. To overcome this defect of spheric gold nanoparticles, there are two methods to make gold nanoparticles adapt in vivo imaging: i) changing a shape of gold nanoparticles from sphere to rod or cage; ii) changing a component of gold nanoparticles from pure metal to silica core-gold shell.

El-Sayed group prepared and employed Au nanorods conjugated to anti-EGFR antibodies for NIR cancer cell imaging (shown in Figure 1) and selective photothermal therapy (Huang *et al.*, 2006b). Using both of SPR scattering and absorption properties of gold nanorod, Cheng group also have shown that the gold nanorod strongly enhanced fluorescence allowing in vivo imaging using a two-photon NIR excitation scheme (Wang *et al.*, 2005**).** Xia group reported gold nanocages and their applications in biomedical imaging (Chen *et al.*, 2005; Cang *et al.*, 2005; Chen *et al.*, 2007). They synthesized 45 nm gold nanocages and precisely tuned SPR peaks of nanocages to 810 nm to match the center wavelength of laser irradiation for photothermal cancer treatment. The nanocages were easily modified with thiolated PEG and then conjugated with HER2-antibody to target EGFR2 that are overexpressed on the surface of

SK-BR-3 breast cancer cells. Their results showed a good promising for the immuno gold nanocages with a size less than 50 nm as a new class of photothermal therapeutic agents for cancer treatment. Halas group in Rice University designed a nanostructure, nanoshells that are composed of a silica core and a thin layer Au shell to obtain a desirable optical tenability (Fortina *et al.*, 2007). The nanoshells can be designed to possess high SPR scattering and/or absorption in the NIR region to facilitate in vivo applications in optical imaging and therapy. Together with her coworkers, her group has shown that human breast cancer cells incubated with nanoshells possess ability of photothermal damage on exposure to NIR laser light. They injected thiolated PEG-coated silica-Au nanoshells into mice tumors. Low doses of NIR laser light cause high temperature localized in the tumor regions that it is enough to induce irreversible tissue damage. On the contrary, control tissues are exposed to NIR light without nanoshells injections show a very low temperature rise without any tissue damage (Hirsch *et al.*, 2003a). In further experiments on the breast cancer cell lines in vitro, NIR laser photothermal therapy showed more selectively via molecular specific labeling of the caner cells with nanoshells conjugated with antibodies to HER2 (Loo *et al.*, 2005a). Her group did a series of work based on nanoshells imaging including whole immunoassay (Hirsch *et al.*, 2003b; Hirsch *et al.*, 2005), photothermal tumor ablation (Hirsch *et al.*, 2003a; O'Neal *et al.*, 2004), cancer imaging (Loo *et al.*, 2004; Loo *et al.*, 2005a; Loo *et al.*, 2005b; Fu *et al.*, 2008), and tissue welding (Gobin *et al.*, 2005) so on.

Comparing to gold nanoparticles, applications of silver nanoparticles in biological and medical imaging are few. Here we list two cases. One case is from Dickson group who employed a strongly emissive individual DNA-coated Ag nanoparticles as single-molecule fluorophores in NIR region. It offers great potential in pushing in vitro or in vivo single molecule studies in future (Vosch *et al.*, 2007). Another

case was from Xu and her colleagues (Xu et al. 2004,). Very recently, their group have directly characterized the transport of single silver nanoparticles into an in vivo model system-zebrafish embryo and investigated their effects on early embryonic development at single-nanoparticle resolution in real time (shown in Figure 2). They found that single Ag nanoparticles (5–46 nm) are transported into and out of embryos through chorion pore canals (CPCs) and exhibit Brownian diffusion (not active transport), with the diffusion coefficient inside the chorionic space around 26 times lower than that in egg water. In contrast, silver nanoparticles were trapped inside CPCs and the inner mass of the embryos, showing restricted diffusion. Their results showed that the biocompatibility and toxicity of Ag nanoparticles and types of abnormalities observed in zebrafish are highly dependent on the dose of Ag nanoparticles, with a critical concentration of 0.19 nM. Unlike other chemicals, single silver nanoparticles can be directly imaged inside developing embryos at nanometer spatial resolution, offering new opportunities to unravel the related pathways that lead to the abnormalities in biological and medical imaging (Lee *et al.*, 2007a).

2) Quantum Dots (QDs) and Hard-Soft Nanoparticles Based on QDs

In comparing with metal nanoparticles, QDs have two biological windows exist for optical imaging in living subjects, one at 700-900 nm and another at 1200-1600 nm. QDs are an ideal candidate for multiple photons imaging in live animal models. In 1998, two groups simultaneously reported their demonstrations of QDs-based utilization in biological and medical imaging applications (Bruchez *et al.*, 1998; Chan *et al.*, 1998). Since then QDs have been linked to some biomolecules such as peptides (Biju *et al.*, 2007), antibodies (Goldman *et al.*, 2002a; Goldman *et al.*, 2002b; Lidke *et al.*, 2004; Winter *et al.*, 2001), streptavidin (Dahan *et al.*, 2003; Wu *et al.*, 2003), nucleic acids (Mahtab et al., 2000), epidermal growth factor (EGF) (Lidke *et al.*, 2004; Derfus *et al.*, 2004a), and other ligands (Rosenthal *et al.*, 2002)

for fluorescent imaging applications. Some excellent review papers on the use of QD nanocrystals for biological labeling, detection and imaging are summarized (Alivisatos, 2004; Chan *et al.*, 2002; Nie *et al.*, 2007).

Another subject for applications of quantum dots is that quantum dots have been tested in fixed cells over the last few years. QDs conjugated with some signal peptides or transfect agents enable to transport biomacromolecules to the assigned organelle in living cells. Hoshino *et al.* have used oligopeptides to penetrate the cellular membrane utilizing their protein transduction domains and to locate their specific organelle (Hoshino *et al.*, 2004a). Derfus and coworkers utilized electroporation or transfection reagents conjugated with QDs to cross cell membrane and track their organelles (Derfus *et al.* 2004b). Up to date, there have been no real successful cases to overcome this complication. The best way for cytoplasmic translocation of QDs is still a direct injection in living. This method allows the targeting of QDs to sub-cellular compartments such as mitochondria or the nucleus using targeting peptides (Chen & Gerion, 2004). However the cell injection, though it is useful for single-cell observation, is tedious work when many cells are to be labeled. A method that makes QDs are homogenously distributed in the cytoplasm of cells would be great expecting. Moreover, Parak *et al.* reported that QDs could be used as a reagent of imaging of phagokinetic tracks in cells (Parak *et al.*, 2002). Two groups also studied used QDs to label live cells and have demonstrated their use for long-term multicolor imaging of live cells (Jaiswal *et al.*, 2002; Hoshino *et al.*, 2004b). As for more details, an excellent review on the synthesis, solubilization, and functionalization of QDs and their applications to cell and animal biology is also available (Michalet *et al.*, 2005). These published results suggested that fluorescent probes of QDs not only are useful as

imaging tools for tracing target cells but also keep a long time in vivo. This is very helpful for living animal experiments.

There is some progress in animal's experiments concerning to QDs due to a rapid development of the synthesis, solubilization, and functionalization of QDs during the last several years. The first animal report on using peptide-QD conjugates to target receptors on blood vessels with exquisite binding specificity was investigated by Ruoslahti group (Akerman *et al.*, 2002). In their pioneer work, ex vivo histological data showed that QDs-Peptide conjugates were specifically directed to a tumor vasculature and other targets. A study reported the first experiment using near infrared QDs in animal surgical procedures in vivo that was presented by Kim et al. in 2004 (Kim *et al.*, 2004). It is a good example of using QDs in medical applications because they first discovered that near-infrared-emitting type-II QDs is able to work in vivo fluorescence imaging of lymph nodes at up to 1 cm depth. At the same year, Nie group reported a new class of multifunctional QD probes for simultaneous tumor targeting and imaging in live animal models (shown in Figure 3) (Gao *et al.*, 2004). Recently, Cai *et al.* studied the in vivo specific targeted imaging of tumor vasculature using QD705-RGD conjugates (Cai *et al.*, 2006). At this moment it is not realistic that QDs-based in vivo imagings in small animal models directly graft to patients because of (i) a limited optical signal penetration depth, (ii) the concerned toxicity of QDs, (iii) poor delivery, and (iv) lack of quantification.

3) Titanium Dioxide

Titanium dioxide nanoparticles are for biological and medical imaging at this time from two laboratories. One is from Woloschak group and another group is Cheon's group. In Woloschak laboratory, they have

shown the effects of TiO_2 nanoparticels conjugating oligonucleotides to the surface of TiO_2 nanoparticles that target different organelles in living cells. X-ray-fluorescence microscopy (XFM) (Paunesku *et al.*, 2006) and TEM data have confirmed that by varying the oligonucleotide sequence bound to the nanoparticle the subcellular localization of the TiO_2-DNA nanoconjugate can change based on the location of available cellular complimentary DNA (Paunesku *et al.*, 2003; Paunesku *et al.*, 2007). Titanium signals were found by XFM and TEM within the nucleus in the cells when breast cancer MCF-7/WS8 cells were treated with TiO_2 nanoconjugates complimentary to genomic DNA encoding 18S rRNA (of which 200–300 copies reside in the nucleolus (Makalowski, 2001.)). On the other hand, both XFM and TEM detected a more disperse Ti signal in the mitochondria throughout the cytoplasm when the oligonucleotide sequence bound to the TiO_2 nanoparticle was complimentary to mitochondrial DNA (shown in Figure 4) (Paunesku *et al.*, 2007). A third experiment showed the combination of XFM and confocal fluorescence microscopy for imaging the same cell treated with a TiO_2-DNA nanoconjugate whose nucleic acid component is labeled with tetramethylrhodamine (TAMRA). It is clearly shown both a titanium signal and fluorescent TAMRA signal in the nucleus as well as in the perinuclear region (Thurn *et al.*, 2007). This result strongly suggested that TiO_2-DNA nanoconjugates were not only penetrate cell membrane and enter cell inside, but also are stable in cells. Moreover, they conjugated TiO_2-DNA with Gd-based compounds to obtain T1-weighted MRI signal that makes a further step toward medical application later (Endres *et al.*, 2007). Cheon group resorted to nanorods of titanium dioxide while Woloschak group used nanospheres of titanium dioxide. Their data clearly showed high photocatalytic effects upon skin-cancer-cell tests using confocal fluorescence microscopy (Seo *et al.*, 2007).

4) Carbon Nanotubes

In 2004, Bianco and coworkers demonstrated for the first time that functionalized carbon nanotubes are able to cross the cell membrane (Pantarotto *et al.*, 2004a). Fluorescent images clearly appeared that carbon nanotubes are a promising carrier system in drug delivery and targeting therapy and act as nanovehicles and evaluating the biological functions of the covalently linked molecules after cellular uptake. The single-walled nanotubes (SWNTs) according to confocal fluorescent imaging are found to across the cell membrane via endocytosis to deliver molecular cargoes including therapy agents (Murakami *et al.* 2004; Bianco *et al.*, 2005; Cai *et al.*, 2005; Zhu *et al.*, 2005), lipids (Singh *et al.*, 2006), near infrared agents (Cherukuri *et al.*, 2004; Kam *et al.*, 2005), peptides (Pantarotto *et al.*, 2003; Pantarotto *et al.*, 2004a), proteins (Kam *et al.*, 2004; Kam & Dai, 2005) and nucleic acids such as plasmids DNA (Pantarotto *et al.* 2004b; Liu *et al.*, 2005; Singh *et al.*, 2005), RNA (Lu *et al.*, 2004) and short interfering RNA (siRNA) (Kam, Liu & Dai, 2005). To investigate a mechanism of SWNTs penetrating the cells and its toxicity, Porter *et al.* showed that it is possible to map the location of intracellular SWNTs using TEM and confocal microscopy (Porter *et al.*, 2007). They successfully imaged individual SWNTs within lysosomes and also crossing cell membranes. They demonstrated two possible pathways of entry of SWNTs into cells: energy-dependent phagocytosis or endocytosis and passive diffusion across lipid bilayers. They showed that direct imaging of SWNTs within cells is achievable and is essential to complement cytotoxicity assays to understand localized. Moreover, Cherukuri *et al.* recent rabbit study used NIR fluorescence to monitor SWNT pharmacokinetics following intravenous administration showed that nanotube fluorescence is also being used in novel biomedical research (shown in Figure 5) (Cherukuri *et al.*, 2006). As a step toward developing biomedical applications based on nanotube fluorescence, Leeuw and colleagues have explored the effects and fate of SWNTs orally

administered to Drosophila melanogaster, the preeminent model organism of biology (Leeuw *et al.*, 2007). This is a demonstration of nanotube imaging within a living organism. Moreover, two groups disclosed articles on the biodistribution of chemically functionalized carbon nanotubes intravenously injected into animals based on biological imaging (Wang *et al.*, 2004; Singh *et al.*, 2006). Both of these two groups reported that SWNTs using various functionanlized methods behaved like small molecules in mice and freely cleaned through the urine with little uptake by the liver, kidney, lung, muscle, skin, spleen, blood, bone, and heart of the reticuloendothelial system (RES).

5) Other Hard or Hard-Soft Nanoparticles

(1) Silica-based nanoparticles

Silica-based nanoparticles are widely used in bioanalytics and biological/medical imaging because they show less aggregation, little dye leakage, easily and versatile ways for surface functionalization and great photostability (Kim *et al.*, 1999; Smith *et al.*, 2006; Tan *et al.*, 2004a). A variety of types of targets such as proteins, cells, and bacteria, have been detected by these silica nanoparticles (Wang *et al.*, 2005; Santra *et al.*, 2001; Houser 1990; Deng *et al.*, 2006; Tan *et al.*, 2004b; Zhao *et al.*, 2004; He *et al.*, 2004). For example, using a covalent bond Santra *et al.* (Santra *et al.*, 2001) attached mouse antihuman CD10 antibody to surface-modified, Rubpy-doped silica nanoparticles and then incubated with mononuclear lymphoid target cells. It confirmed that the effectiveness of this method to detect leukemia cells selectively. Another case was that Deng and coworkers (Deng *et al.*, 2006) doped the silica matrix using a near-infrared fluorescent dye, methylene blue. NIR imaging showed that the doped silica nanoparticles conjugated with monoclonal anti-alpha fetoprotein, AFP (a type of cancer marker) antibody is possible to make fluorescence-anisotropy measurements directly on whole blood samples. The Eu-doped silica

nanoparticles were also used for targeting of human squamous cancer cells (SCC-9) and imaging with confocal fluorescent microscopy (Santra *et al.*, 2005).

(2) Diamond nanoparticles (Nanodiamond)

Nanodiamond is superior in physical and biocompatible properties. It has emerged as a promising material for biomedical applications. For example, fluorescent nanodiamonds with 35-100 nm are stable biomarkers in bioimaging (Narayan *et al.*, 2006; Yu *et al.*, 2005; Fu *et al.*, 2007). Very recently, Ho and coworkers attached an anticancer agent-doxorubicin hydrochloride (DOX) for therapeutic delivery confirmed by optical imaging results (Huang *et al.*, 2007).

III. Nanoparticles for CT

Nanoparticels contribute to CT concentrated on iodine/surfactant-based liposome soft nanoparticles (Thomsen & Morcos, 2000), gadolinium-based liposome soft nanoparticles (Henson *et al.*, 2004; Chryssidis, Davies & Tie 2002; Quinn *et al.*, 1994), barium sulphate hard nanoparticles, and newly appeared metallofullerenes hard nanoparticles (Miyamoto *et al.*, 2006), gold hard nanoparticles (Hainfeld *et al.*, 2006; Kannan *et al.*, 2006; Kattumuri *et al.*, 2007; Kim *et al.*, 2007; Cai *et al.*, 2007a) and bismuth sulfide hard nanoparticles (Rabin *et al.*, 2006). Barium sulfate was used as a contrast agent to improve the visualization of the gastrointestinal tract in an x-ray image instead of barium sulfide since 1920s (Patton, 1994). The iodine-based liposome soft nanoparticles are divided into ionic and non-ionic contrast media depending on the iodine-type in compounds (Thomsen & Morcos, 2000). As for metallofullerenes, gold nanoparticles and bismuth sulfide nanoparticles, there are just appeared and no applications now in

clinics yet comparing with barium sulfate and iodinated agents that have been approved by FDA for many years.

A very unique example is that Miyamoto *et al.* reported a method on aqueous soluble metallofullerenes as CT contrast agents (Miyamoto *et al.*, 2006). Furthermore, Hainfeld *et al.* studied gold nanoparticles without modification as a new CT contrast agent and applied to a mice model (Hainfeld *et al.*, 2006), two groups used polymer-modified gold nanoparticles as CT contrast agents (Kim *et al.*, 2007; Cai *et al.*, 2007a) while Katti and his group are developing a CT contrast agent based on nontoxic phytochemical gum-arabic matrix coating gold to increase the concentration of gold nanoparticles and gold isotope 198 to attain therapy purpose in future (Kannan *et al.*, 2006; Kattumuri, *et al.*, 2007). It should be noted that measurement of the X-ray absorption coefficient in vitro revealed that the attenuation of different PEG-gold nanoparticles is over five times higher than that of the current iodine-based CT contrast agent (shown in Figure 6) (Kim *et al.*, 2007).

Mukundan and coworkers used liposomal iodinated nanoparticles for preclinical CT in mice model (Mukundan *et al.*, 2006). Mcintire *et al.* investigated in detail four types of iodinated nanoparticles in rabbit lymph nodes after subcutaneous injection (Mcintire *et al.*, 2000). They found that 1) all four agents provided adequate enhancement of both the popliteal and axillary lymph nodes of the rabbit (ie, > [DELTA]100 HU). 2) Lymph node volume appears to be related to clearance of insoluble, iodinated nanoparticle contrast agents from lymph nodes can be modulated by changes in the structure of the agent itself. 3) Using the same agent, smaller particles deliver material to the lymph nodes more quickly and clear more quickly. Hyafil and colleagues studied that macrophages in atherosclerotic plaques of rabbits

can be detected with a clinical X-ray computed tomography (CT) scanner after the intravenous injection of a contrast agent formed of iodinated nanoparticles-N1177 dispersed with surfactant. This contrast agent may become a key adjunct to the clinical evaluation of coronary arteries with CT (shown in Figure 7) (Hyafil *et al.*, 2007). Kao *et al.* tested liposomal iohexol nanoparticles that the liposomal iohexol formulation had a sufficient residence time for blood pool imaging in a rabbit model (Kao *et al.*, 2003). The further experiments with long-residence-time iohexol formulations might lead eventually to applications in cardiac imaging and in early tumor detection. Suga *et al.* investigated that a quick and accurate localization of sentinel lymph node station on detailed underlying lung anatomy by using indirect computed tomographic lymphography (CT-LG) may be of value to guide selective lymph node dissection for minimally invasive surgery in non-small cell lung cancer (Suga *et al.*, 2004). Wisner and coworkers found that a surface-modified, iodinated chylomicron remnant-like emulsion provided marked, selective enhancement of targeted lymph nodes after subcutaneous administration (Wisner *et al.*, 2002). Moreover, the formulation produced significant opacification of more distant node groups from a single injection. Wolf and coworkers estimated in vivo extraction of lymphographic material in the popliteal node of the rabbit using radiopaque nanoparticles (Wolf *et al.*, 1999). Gazelle *et al.* evaluated the efficacy of a nanoparticulate computed tomography (CT) contrast agent-Ethyl ester of diatrizoic acid (EEDA) in an animal model of focal liver disease (Gazelle *et al.*, 1995). They found that liver-directed agent such as EEDA may prove to be more efficacious than currently available extracellular agents designed for liver CT scanning. Wisner *et al.* also evaluated the imaging characteristics of an iodinated particulate contrast agent for indirect computed tomography (CT) lymphography of normal subdiaphragmatic lymph nodes in dogs (Wisner *et al.*, 1995). The CT images showed enhancement of regional lymph nodes draining at various injection sites.

There are still other applications for different nanoparticles as contrast agents of CT. The interested ones can refer to excellent reviews on potential CT-contrast media (Yu & Watson, 1999) and newly present contrast agents (Blankenberg, 2003).

IV. Nanoparticles for MRI

Nanoparticles as contrast agents for MRI have benefited for medical examinations a lot because sometimes T1-wighted, T2-weighted or T2*-weighted images by themselves in the tissues do not adequately show the anatomy or pathology. The frequently used Gd-liposome (Mulder *et al.*, 2006.), Gd-polymer (Kobayashi & Brechbiel, 2005), Gd-DNA (Endres *et al.*, 2007), and Gd-protein (Chan & Wong, 2007) based soft nanoparticles are T1- enhanced contrast agents in MRI while iron oxide (Mulder *et al.*, 2007) or other (super-) paramagnetic hard nanoparticles (Seo *et al.*, 2006; Babinec & Babincová, 2007) usually act as a T2, particularly T2* enhanced contrast agents. It should be noted that when the small size of iron oxide or other supermagnetic hard nanoparticles may enhance T1 signal as well as enhancements of T2 and T2* (Cunningham *et al.*, 2005; Mani *et al.*, 2006). A summary for the different contrast agents for MRI is shown in Table 2.

1) T1-contrast agents for MRI

T1 contrast agents based on Gd components were first introduced in MRI by Young *et al.* after Levy and coworkers confirmed that there is an enhancement in magnetic resonance field (Levy, Dechter, & Kowalewski, 1978; Young *et al.* 1981; Carr *et al.* 1984). Gadolinium-based MRI contrast agents (CAs)

of various sizes and chemical properties prepared via relatively simple chemistry are capable of offering sufficient contrast enhancement for various applications (Kobayashi & Brechbiel, 2005). First as to the different sizes of the contrast agents based Gd components, they show different functions for examples 1) A small sized polyamidoamine (PAMAM) dendrimer-core based <3 nm contrast agents are easy to leak across the vascular wall causing rapid perfusion; 2) 3-6 nm of contrast agents are quickly excreted through the kidney that show a good promising in functional renal contrast enhancements; 3) 7-12 nm of contrast agents enable to use as blood pool contrast agents because there are retained in circulation; 4) 12-15 nm of contrast agents are easy to recognize by the reticulpendothelial system (RES) not by the vascular walls or excretion routes; and 5) 15-20 nm of contrast agents act differently behaviors in the body. Moreover, as to different chemical properties, the contrast agents based on Gd-components also show various functions such as 1) contrast agents having a hydrophobic core of with polypropylenimine diaminobutane (DAB) dendrimer are easy to accumulate in the liver and used as liver contrast agents; and 2) hydrophilic contrast agents can be used for lymphatic imaging. Finally, contrast agents targeted either antibodies (Sipkins *et al.*, 1998), receptors (Lipinski *et al.*, 2006), DNA (Endres *et al.*, 2007), or functional peptides (Tesauro *et al.*, 2007) can act as tumor-specificity agents with a dual diagnostic and therapeutic functions (Winter *et al.*, 2006) based on gadolinium component (Kobayashi & Brechbiel, 2005; Lee *et al.*, 2007b).

The Gd-based agents have a good many applications as MRI contrast agents for imaging functional anatomy of tumor blood vessels such as contrast agents for Micro-MR angiography of normal and intratumoral vessels (Kobayashi *et al.*, 2001a), contrast agent for detection of alterations of tumor vessel permeability induced by radiation (Kobayashi *et al.*, 2004a); specific organs such as liver (Kobayashi *et*

al., 2001b), kidney (Kobayashi *et al.*, 2002; Kobayashi *et al.*, 2004b), brain (Ito *et al.*, 2006); and the lymphatic nodes system (Kobayashi *et al.*, 2003; Kobayashi *et al.*, 2006). The previous results of liver, kidney targeting, or lymphatic, particularly sentinel node imagings (Kobayashi *et al.*, 2004c) showed that the Gd-based contrast agents have been applied to further pre-clinical studies or clinical practices (Kobayashi & Brechbiel, 2005; Laurent, Vander Elst & Muller, 2006; Xu *et al.*, 2007).

An exceptional case of T-1 contrast agents based on gadolinium is Gd_2O_3 solid nanopartricles (Burnett *et al.*, 1985; Bridot *et al.*, 2007). These luminescent hybrid nanoparticles of Gd_2O_3 coated a layer of polysioxane shell that includes organic fluorophores and carboxylated PEG covalently immobilized on the surfaces of the inorganic nanoparticles. The experimental data showed that these particles induce an enhancement of the positive contrast of MRI as compared to the generally used positive contrast agents like Gd-DOTA in clinical MRI practices (shown in Figure 8). These solid T1 nanoparticles may also have good promising in diagnostic and neutron-capture therapy.

2) T2-contrast agents for MRI

T2/T2* contrast agents first developed by Lauterbur group in 1983 and then they and other groups used superparamagnetic particles for MRI (Mendonca-Dias, Gaggelli & Lauterbur, 1983; Lauffer *et al.*, 1985; Mendoca-Dias & Lauterbur 1986; Saini *et al.*, 1987; Stark *et al.*, 1988; Corot *et al.*, 2006). The currently used ultrasmall superparamagnetic iron-oxide nanoparticles for T2/T2* contrast agents was introduced by Weissleder and coworkers in 1990 (Weissleder *et al.*, 1990a). USPIOs usually have cores of 4-6 nm with hydrated dynamic particle diameters of 10-40 nm (Wang, Hussain & Krestin, 2001; Wu, Tang & Jensen, 2004). The (U)SPIOs generally produce very strong transverse and longitudinal relaxation effects in vivo

compared with Gd-based contrast agents (Corot *et al.*, 2006). For instance, a dose of 7 μmol iron/kg of a USPIO agent (NC100150) yielded a signal drop almost equal to that of a standard 0.2 mmol/kg gadodiamide injection in bolus tracking measurement of cerebral blood volume (CBV) and cerebral blood flow (CBF) (Simonsen *et al.*, 1999; Wu, Tang & Jensen 2004). Up to date, the (U)SPIO nanoparticles via targeted or non-targeted ways have been widely used in differently biological or clinical applications such as imaging of targeted of small molecules (Weissleder *et al.*, 2005), targeted-receptors (Weissleder *et al.*, 1991), magnetically labeled cells (Schulze *et al.*, 1995), cell migration (Lewin *et al.*, 2000), atherosclerotic plaque (Kooi *et al.*, 2003; Frias *et al.*, 2004), cell inflammation (Dunn *et al.*, 2005), tissue inflammation (Turvey *et al.*, 2005), reticuloendothelial systems (RES) (Chavanpatil, Khdair & Panyam, 2006) including liver (Harisinghani *et al.*, 2001), spleen (Ferrucci & Stark, 1990; Kim *et al.*, 2006)), and lymph nodes (Weissleder *et al.*, 1990b; Harisinghani *et al.*, 2003); perfusion imaging of brain (Enochs *et al.*, 1999), myocardium (Weissleder *et al.*, 1992), and kidney (Grenier, Pedersen & Hauger, 2006); MR angiography (Barrett *et al.*, 2006; Warmuth *et al.*, 2007); and tumor vascular imaging (Bentzen *et al.*, 2005).

At present the nanoparticles for biomedical imaging applications of T2 contrast agents in animal models in published documents are few such as Dai group reported that FeCo core/single graphitic-shell nanoparticles (Seo *et al.*, 2006) and Cheon group discovered spinel ferrite nanoparticles (Lee *et al.*, 2007c)) besides USPIOs and SPIOs. Dai group found that FeCo/C core-shell nanoparticles show ultrahigh saturation magnetization and r1/r2 relaxivities. A preliminary in vivo result demonstrated long-lasting positive contrast enhancement for vascular MRI in a rabbit model. This core-shell nanoparticle may as a combined agent for integrated diagnosis and therapeutic applications. Cheon group used

artificial engineering methods to prepare the spinel ferrite nanoparticles and conjugated with antibodies that showed an enhancement of T2 signal for the detection of cancer markers compared with normal used probes. Also they successfully visualized small tumors in a mouse model (shown in Figure 9). These high-performance magnetic nanoparticle systems could play a key role in the real-time imaging of biological/medical events for example cell trafficking, cancer metastasis, cellular signaling and tumor diagnostics so on.

3) A combination of T1 and T2-contrast agents for MRI

Some groups tested a combination of T1-weighted and T2-weighted images simultaneously in MRI. Burnett and coworkers demonstrated the utility of gadolinium oxide (Gd_2O_3) nanoparticles as a liver, spleen, and lung-contrast enhancing agent with marked increase in signal intensity in both T1 and T2 relaxation acceleration at even small quantities (Burnett *et al.*, 1985). Morover, Chapon *et al.* showed that it is possible to make an accurate characterization of myocardial infarction volume and to detect myocardial viability post-infarction in rats (Chapon *et al.*, 2005). Yuan *et al.* have identified lipid-rich necrotic core with 85% sensitivity and 92% specificity in advanced human carotid arteries using multi-contrast techniques in vivo MRI (Yuan *et al.*, 2001). Benefiting from a combination of multiple contrast techniques, it is possible to recognize plaque anatomy and its fine structures or even if compositions in animal models (Skinner *et al.*, 1995; Helft *et al.*, 2001), distinguish the aorta (Fayad *et al.*, 2000) and the carotid artery (Toussaint *et al.*, 1996) in the human.

V. Nanoparticles for USG

Ultrasonography (ultrasound imaging) by tissues and borders between tissues is mainly relied on a difference between the products of the speed of sound in the medium multiplied by the density of that medium i.e. an acoustic impedance mismatch (Leighton, 1997). Contrast agent particles with a highest echo response would be the ones that imply the highest acoustic impedance mismatch between the bulk mediums for example blood that has acoustic impedance quite close to water and a microphase composed of contrast agents. Several kinds of contrast agents in ultrasound imaging based on nanoparticles/ microparticles include hard nanoparticles such as solid silica/polymer nanoparticles (Liu et al., 2006; Liu et al., 2007a), metal oxide nanoparticles (Nolte *et al.*, 2005) and noble metal nanoparticles (Willard & Van Bommel, 2005), and soft nanoparticles such as liquid-core microemulsions and nanoemulsions (Lanza *et al.*, 1996), liposomes (Alkan-Onyuksel *et al.*, 1996), and gas-filled microbubbles with the average size of several micrometers (Fritz *et al.*, 1997; Meza *et al.*, 1996). The hard nanoparticles used for ultrasound imaging is their preliminary phase and few studies concerned. We will not discuss in detail. Within the soft nanoparticles/microparticles contrast agents, the gas-filled microbubble provides the highest contrast signal in ultrasound imaging (Klibanov *et al.*, 2002). The liquid contrast emulsion nanoparticle/microparticle shows a lower contrast signal but enhanced stability and prolonged circulation time (Lanza *et al.*, 1996). As for the multilamellar liposome-based agents, they were initially supposed to offer different acoustic responses due to their multilamellar lipid structures (Alkan-Onyuksel *et al.*, 1996); later, the studies showed that their acoustic responses was caused by incorporated pockets of gas phase (Huang *et al.*, 2002). A signal enhancement by the liposome particles provided is several orders of magnitude lower than that of microbubble-based agents (Coussios *et al.*, 2004; Klibanov, 2005). Since the microbubbles show the best detection sensitivity and some of those contrast agents are already

approved for blood pool indications by FDA, herein we will focus on the discussion of the microbubble-based contrast media in ultrasound imaging applications.

Gramiak and Shah first showed that the gas microbubbles were able to use to enhance ultrasound contrast in 1968 (Gramiak & Shah, 1968). Usually the gas microbubbles need to coat a layer of stuffs or target some receptors or ligands to be suitable for a stable and specific contrast agent in ultrasound imaging. In the 1980s, ultrasound contrast agents were coated with an adsorbed layer of saccharide (Feinstein *et al.*, 1984) or protein (Feinstein *et al.*, 1990). The albumin-coated microbubbles such as Albunex® and Optison™ (GE Healthcare) were the first commercially available and FDA-approved contrast agents. The first successful targeted ultrasound contrast agents were developed in the late 1990s using avidin-biotin adhesion (Lanza *et al.*, 1997; Klibanov, 1999). For in vivo imaging, a three-step process was developed by Lanza group (Lanza *et al.*, 1997). Step one, a biotinylated monoclonal antibody was administered and bound to fibrin within the clot. Step two, Avidin molecules were administered that bound the biotin on the monoclonal antibody. Step three, biotinylated ultrasound contrast agents were given that bound the exposed end of the avidin molecule. This targeting ultrasound contrast caused a four-fold increase in acoustic signal from clots (Lanza *et al.*, 1997). Up to date, the various targeted ultrasound probes such as ICAM1 (Song *et al.*, 2002), VCAM1 (Hamilton *et al.*, 2004), P-selectin (Lindner *et al.*, 2001), fibrin (Lanza *et al.*, 1997; Demos *et al.*, 1999), avidin (Korpanty et al., 2005), genetic payloads (Frenkel *et al.*, 2002; Lentacker *et al.*, 2006), and integrins (Leong-Poi *et al.*, 2003) have been successfully tested. In clinical ultrasound systems these stabilized microbubbles have been used to enhance the reflectivity of perfused tissues in applications spanning cardiology, neuroscience, and radiology. The targeted contrast agents have not yet been applied clinically (Sakamoto *et al.*, 2005; Kruger Hagen *et al.*, 2000), but

preclinical studies have successful demonstrated application in angiogenesis and vascular inflammation besides these microbubbles may be good candidates for targeted delivery of therapeutic agents. As for the details of contrast agents in ultrsoungraphy, the interested readers please refer to an outstanding review written by Ferrara *et al.* (Ferrara, Pollard & Borden, 2007).

VI. Nanoparticles for PET

In PET, the radiolabled nuclides are conjugated to receptors, enzymes, transporters, ion channels, siRNA, mRNA, and specific substrate-associated sites such as β-amyloid plaques found in Alzheimer's disease to form soft nanoparticles (Collier *et al.*, 2002; Groves *et al.*, 2007; Holschbach & Olsson, 2002; Jarkas *et al.*, 2005; Wilson *et al.*, 2002). The radiolabled nuclides are also attached to the surfaces of some hard nanoparticles such as carbon nanotubes (Liu *et al.*, 2007b). The generally used positron-emitting radionuclides are ^{11}C ($t_{1/2}$=20.4 min), ^{13}N ($t_{1/2}$=9.96 min), ^{15}O ($t_{1/2}$=2.03 min), ^{18}F ($t_{1/2}$=109.8 min), ^{64}Cu ($t_{1/2}$=12.7 hours), ^{68}Ga ($t_{1/2}$=68 min), ^{76}Br ($t_{1/2}$=16.1 hours), ^{86}Y ($t_{1/2}$=14.7 hours), ^{89}Zr ($t_{1/2}$=3.3 days), ^{94m}Tc ($t_{1/2}$=52.5 min), ^{94}Tc ($t_{1/2}$=293 min), ^{124}I ($t_{1/2}$=4.3 days), and ^{177}Lu ($t_{1/2}$=6.7 days) (Roeda *et al.*, 2007; Räty *et al.*, 2007; Barker *et al.*, 2001; Cai, Niu & Chen, 2007). Depending on these radionuclides injected, many biologic and metabolic processes such as glucose metabolism (^{18}F-deoxyglucose (18-FDG)), DNA synthesis (^{11}C-thymidine) and consumption (^{18}F-thymidine (18-FLT)), amino acid transport and metabolism (^{11}C-methionine) in cell, ER expression (^{18}F-16α-fluorestradiol (FES)), bone formation and mineralization (^{18}F-fluoride), thymidine kinase activity (^{18}F-fluorothymidine (FLT)), blood flow and perfusion ($H_2{}^{15}O$, ^{82}Rubidium, and $^{13}NH_3$), or tissue hypoxia (^{18}F-misonidazole) can be visualized using PET (Machtens *et al.*, 2007; Långström, Itsenko & Rahman, 2007; Mankoff & Eubank, 2006).

Among these radionuclides, ^{18}F specially 18-fluorodeoxyglucose ([^{18}F]FDG) is the most widely used tracer in oncology and clinical diagnosis and many review papers appeared for this kind of agent (de Geus-Oei *et al.*, 2007; Ido *et al.*, 1978; Nutt, 2007; Vallabhajosula, 2007). Herein, we want to show some cases for ^{64}Cu-labeled nanoparticles in PET. Pressly *et al.* reported ^{64}Cu-labeled nanoparticles comprised of amphiphilic block graft copolymers and tried studing the pharmacokinetics and enhanced blood lifetime based on the labeled nanoparticles (Pressly *et al.*, 2007). Dai and Chen groups co-investigated the biodistribution of ^{64}Cu-labelled SWNTs in mice by in vivo PET, ex vivo biodistribution and Raman spectroscopy (Liu *et al.*, 2007b). It is found that effectively PEGylated SWNTs show relatively long blood circulation time and low uptake by the reticuloendothelial system (RES) and a high tumour accumulation (shown in Figure 10). Sun *et al.* developed a novel strategy to construct shell crosslinked nanoparticles with large numbers of DOTAlysines per particle (> 400) that were accessible for ^{64}Cu radiolabeling. It showed good promosing in vivo PET tracers at low administering doses (Sun *et al.*, 2007). Davis group conjugated 1,4,7,10-tetraazacyclododecane-1,4,7,10-tetraacetic acid to the 5' end of the targeted siRNA nanoparticles and allowed labeling with ^{64}Cu for PET imaging. They found that transferrin-targeted siRNA nanoparticles reduce tumor luciferase activity by 50% relative to nontargeted siRNA nanoparticles 1 d after injection (Bartlett *et al.*, 2007). Chakrabarti *et al.* imaged oncogene mRNAs with radiolabel-^{64}Cu PNA-peptide nanoparticles by PET and found the targeted nanoparticles provide specific oncogene expression in pancreas cancer xenografts (Chakrabarti *et al.*, 2007).

VII. Nanoparticles for Multimodality Imaging

Among all biological and medical imaging modalities, there is no single modality perfect and sufficient to obtain all the necessary information (Massoud & Gambhir, 2003). For instance, it is difficult to accurately quantify optical signals in living subjects, especially in deep tissues; MRI suffers from low sensitivity with high resolution; Radionuclide-based imaging techniques such as PET and SPECT have very high sensitivity with relatively poor resolution. USG offers a very cheap and facilitable method, but the resolution is also poor and no way for hard tissues. CT with high resolution is concerned because of an exposure under the x-ray for the patients in clinical diagnosis. A combination of multiple biological and medical imaging modalities can provide many advantages over any modality alone. One hand, combining optical imaging with 3D tomographic techniques such as PET, CT including SPECT, or MRI can allow for noninvasive imaging in vivo with higher sensitivity and/or accuracy. On the other hand, various nanoparticles with large surface areas where multiple functional unites can be incorporated for multimodality imaging (Cai & Chen, 2007; Stell *et al.*, 2007).

(1) MRI & Optical Imaging

Several groups used various magnetic nanoparticles to conjugate optical activity components for magnetic-opto bimodal imaging (Talanov *et al.*, 2006; Neuwelt *et al.*, 2004; Veiseh *et al.*, 2005). The Cy5.5–PEG–iron oxide soft-hard nanoparticles were coated with clorotoxin, a glioma tumor-targeting peptide made of 36-amino acids in order to improve tumor-specific binding of multimodal imaging probes (Kircher *et al.*, 2003; Veiseh *et al.*, 2005). A cellular uptake study of 9L glioma cells (positive control) and rat cardiomyocyte (rCM) cells (negative control) showed tumor-specific binding and internalization of the targeted nanoparticles by glioma cells. Choi *et al*. conjugated magnetic iron oxide nanoparticles with near-infrared (NIR) fluorescent single-walled carbon nanotubes (SWNT) forming

heterostructured complexes that can be used as bimodal bioimaging agents (Choi *et al.*, 2007). These nanoparticulate complexes have a longer spin-spin relaxation time than typical ferromagnetic particles due to the smaller size of their magnetic component while still retaining SWNT optical signals. The DNA-wrapped nanoparticulate complexes uptaked by macrophage cells were imaged using MRI and NIR mapping. It demonstrated that these multifunctional nanostructures could potentially be useful in multimodal biomedical imaging. Hilger group using fluorescent magnetosomes bimodal contrast agent for diagnostic purposes shows an excellent spatial resolution of the MRI and the high sensitivity of the fluorescence imaging (Lisy *et al.*, 2007). Yang *et al.* reported Gd(III)-functionalized fluorescent quantum dots as multimodal imaging probes (Yang *et al.*, 2006). These multimodal probes exhibit yellow fluorescence and strong paramagnetism signal. Van Tilborg *et al.* using Annexin A5-conjugated magnetic nanoparticules showed significantly increasing the relaxation rates of apoptotic cell pellets compared to untreated control cells and apoptotic cells that were treated with nonconjugated nanoparticles (van Tilborg *et al.*, 2006). Moreover, Jaffer *et al.* studies showed that atherosclerosis-targeted magnetic nanoparticles provide a foundation for using them to image genetic and/or pharmacological perturbations of cellular inflaniniation in atherosclerosis by MRI and optical imaging (Jaffer *et al.*, 2006).

(2) MRI & SPECT/CT

Zheng *et al.* evaluated the *in vivo* performance of a liposome formulation that co-encapsulates iohexol and gadoteridol as a bimodal contrast agent for CT and MR-based image guidance applications (Zheng *et al.*, 2007). The long *in vivo* circulation lifetime and simultaneous CT and MR signal enhancement provided by this liposome system make it a good candidate for image guidance applications. Watkin *et al.* synthesized gadolinium oxide albumin microspheres (GOAM) and have been able to conduct some

preliminary imaging studies utilizing ultrasound, MR and CT. (Watkin *et al.*, 2002). Zielhuis *et al.* synthesized nanosized liposomes were designed and labeled with the radionuclides, holmium-166 (both a beta- and gamma-emitter and also highly paramagnetic) or technetium-99m, and coloaded with paramagnetic gadolinium allowing multimodal SPECT and MR imaging and radionuclide therapy within one single agent. These nanoparticulate liposomes allow for multimodality imaging and therapy, which makes these new agents highly attractive for future applications (Zielhuis *et al.*, 2006).

(3) MRI & Ultrasound Imaging

Nolte *et al.* evaluated that SPIO particles improved the detection and demarcation of the experimental gliomas on sonograms, which may improve intraoperative neuronavigation with sonography. It might also provide a way to enhance both MRI and US imaging (Nolte *et al.*, 2005).

(4) PET & Optical Imaging

Chen group quantitatively developed a tumor-targeting efficacy of a dual-function QD-based probe with PET and near-infrared fluorescent imaging (Cai *et al.*, 2007b). This dual-function probe has significantly reduced potential toxicity and overcomes the tissue penetration limitation of optical imaging, allowing for quantitative targeted imaging in deep tissue.

(5) PET &CT

Bartlett *et al.* employed PET and CT to monitor whole-body biodistribution kinetics and tumor localization of siRNA nanoparticles while simultaneously using bioluminescent imaging (BLI) to measure luciferase knock down by the delivered siRNA molecules (Bartlett *et al.*, 2007). By formulating

nanoparticles with or without Tf targeting ligands, the effect of cell-specific targeting on both biodistribution and function can be studied simultaneously within the same animal. Antoch *et al.* evaluated that Mannitol-LBG might be used as a negative oral contrast agent at PET/CT scanning because it provides excellent bowel distention while avoiding contrast material–induced PET artifacts (Antoch *et al.*, 2004).

VIII. Perspective

Although molecular imaging and other means can be used to effectively detect small lesions in the human body, how are smaller units, such as atoms, molecules, formed? That is: Where are the boundaries of the atoms in the various biomolecules in the human body? Where are the boundaries of the molecules in the human organelles? Where are the boundaries between cells in human tissues? Where is the boundary between the various organelles in human cells? Where is the boundary between the various tissues in human organs? Where is the boundary between healthy tissues and lesions in the human body, such as tumors and brainwashing vascular diseases? How does the lesion tissue in the human body evolve and migrate? Where is the boundary between the various organs in the human body?

Beyond the human body,Where are the boundaries between people (including physical boundaries and spiritual boundaries, etc.)? Where are the boundaries on land, mountains, lakes and forests (and between the units within them)? Where are the boundaries between groups? Where is the boundary between living and inanimate? Where is the boundary between land and sea on Earth? Where is the boundary between life and death? Where are the borders between countries (including physical and ideological boundaries, etc.)? How are the boundaries between the various units of society divided, changed, evolved and migrated? Where is the boundary between the Earth and the Moon? Where are the boundaries of the solar system? How do the boundaries of all things in nature move, transform and change? How do the units in the universe evolve and change? Where are the boundaries between religions? Where are the boundaries between the various social ideologies? Where are the boundaries of the universe? Where are the boundaries of the Milky Way? Where is the boundary between consciousness and matter? Where is the boundary between philosophy and the natural sciences? When

are the boundaries unclear, and conflicts arise when the boundaries of different systems are blurred between individuals, between social organizations, between nations, between spirit and matter, between galaxies, between host stars and moons, and so on? How to avoid conflicts from the constraints of boundary conditions? Although here we only review the imaging process of various lesions in organisms, especially tumors, by using molecular imaging probes, which can clearly show the boundary between tumors and healthy tissues. However, more boundaries can be considered and more boundarics questions are worth exploring later.

IX. Conclusions

Nanotechnology has contributed to all subjects of general biological and medical imaging fields as we discussed above-mentioned in this review. 1) For optical imaging (OI), different shapes of gold nanoparticles and various types of QDs have been fouced on non-targeted or targeted in vivo/vitro experiments besiedes other nanoparticles. Those results showed a good promising but there is still a long way to reach clinical application because of some concerns for example how to eliminate the toxicity of QDs in the body. 2) For computed tomography, the commercial barium-based hard particles and iodinated-liposomes/micelles nanoparticles have been used to clinical practice for many years though there are still some side effects for the patients. Other types of nanoparticulate materials such as Bi_2S_3 and heavy metal nanoparticles, for example gold nanoparticles are just at the beginning of in vivo experiments. 3) For magnetic resonance imaging, the most well-investigated contrast agents for T1 contrast agent of Gd-based different nanoparticles have been approved by FDA and used in clinic for some years. At the same time, the most used T2 contrast agent of iron oxide nanoparticles have been already in clinical practice or in pahse III-stage clinical trails. 4) For ultrasonography, various microbubbles have been used in clinical practices for many years, but there are few cases for nanosized particles in clinic except there are several lipisome-based nanoparticles in vivo experiments done. 5) For piostron emission tomography, a series of radio-labled nuclei attached to surface of liposome or other

types nanoparticles have been done in vivo or in vitro. 6) Very recently, nanoparticles with multifunctions for the multimodal imaging have appeared. MRI/OI, MRI/SPECT/CT, MRI/USG, PET/OI, and PET/CT have been shown a good promising in vitro, ex vivo, or even in vivo (Cai & Chen, 2007).

In summary, the future of various nanoparticles for biological and medical imaging will be multifunctional, targeted along with therapeutic function (Cai & Chen, 2007). There is good promising in nanoparticles for biological and medical imaging, but there is still a long way to go. The final goal is that nanoparticles-based agents are capable of allowing for efficient, targeted in vivo delivery of therapeutically functional drugs without or very less toxicity for patients as well as the therapy process of patients can be monitored by a non-invasive way over time.

X. Acknowledgements

This work was supported by the National Natural Science Foundation of China (32025021, 31971292, and 32111540257), National Key R&D Program of China (2018YFC0910601, 2019YFA0405603), the Science & Technology Bureau of Ningbo City (2020Z094), and the Key R&D Program of Zhejiang Province (2020C03110). We are also grateful to the Shanghai Synchrotron Radiation Facility (SSRF) in China for their help with the XANES beam Line and National Synchrotron Radiation Laboratory in Hefei, China.

XI. References

Akerman, M.E., Chan, W.C.W., Laakkonen, P., Bhatia, S.N. & Ruoslahti, E. (2002). Nanocrystal targeting in vivo. *Proceedings of the National Academy of Sciences of the United States of America* **99**, 12617-12621.

Alkan-Onyuksel, H., Demos, S. M., Lanza, G. M., Vonesh, M. J., Klegerman, M. E., Kane, B. J., Kuszak, J. & McPherson, D. D. (1996). Development of inherently echogenic liposomes as an ultrasonic contrast agent. *Journal of Pharmaceutical Sciences* **85**, 486-490.

Alivisatos, P. (2004). The use of nanocrystals in biological detection. *Nature. Biotechnology* **22**,47–52.

Antoch, G., Kuehl, H., Kanja, J., Lauenstein, T.C., Schneemann, H., Hauth, E., Jentzen, W., Beyer, T., Goehde, S.C. & Debatin, J.F. (2004). Dual-modality PET/CT scanning with negative oral contrast agent to avoid artifacts: Introduction and evaluation. *Radiology* **230**, 879-885.

Babinec, P. & Babincová, M. (2007). Towards multimodal nanoparticle labels for molecular imaging of biological processes. *Medical Hypotheses*, **69**, 703-704.

Barker, W.C., Szajek, L.P., Green, S.L. & Carson, R.E. (2001). Improved Quantification for Tc-94m PET Imaging. *IEEE Transactions on Nuclear Science* **48(3)**, 739.

Bartlett, D.W., Su, H., Hildebrandt, I.J., Weber, W.A. & Davis, M.E. (2007). Impact of tumor-specific targeting on the biodistribution and efficacy of siRNA nanoparticles measured by multimodality in vivo imaging. *Proceedings of the National Academy of Sciences of the United States of America* **104(39)**, 15549–15554.

Barrett, T., Kobayashi, H., Brechbiel, M. & Choyke, P. L. (2006). Macromolecular MRI contrast agents for imaging tumor angiogenesis. *European Journal of Radiology* **60(3)**, 353-366.

Bentzen, L., Vestergaard-Poulsen, P., Nielsen, T., Overgaard, J., Bjornerud, A., Briley-Saebo, K., Horsman, M.R. & Ostergaard, L. (2005). Intravascular contrast agent-enhanced MRI measuring contrast clearance and tumor blood volume and the effects of vascular modifiers in an experimental tumor. *International Journal of Radiation Oncology Biology Physics* **61(4)**, 1208-1215.

Bethune, D.S., Kiang, C.H., Devries, M.S., Gorman, G., Savoy, R., Vazquez, J. & Beyers, R. (1993). Cobalt-catalyzed growth of carbon nanotubes with single-atomic-layer walls. *Nature* **363(6430)**, 605-607.

Bianco, A., Hoebeke, J., Godefroy, S., Chaloin, O., Pantarotto, D., Briand, J.P., Muller, S., Prato, M. & Partidos, C. D. (2005). Cationic carbon nanotubes bind to CpG oligodeoxynucleotides and enhance their immunostimulatory properties. *Journal of the American Chemical Society* **127**, 58-59.

Biju,V., Muraleedharan, D., Nakayama, K., Shinohara, Y., Itoh, T., Baba, Y., & Ishikawa M. (2007). Quantum dot-insect neuropeptide conjugates for fluorescence imaging, transfection, and nucleus targeting of living cells. *Langmuir* **23(20)**, 10254 –10261.

Blankenberg, F.G. (2003). Molecular imaging: the latest generation of contrast agents and tissue characterization techniques. *Journal of Cellular Biochemistry* **90(3)**, 443-453.

Burnett, K.R., Wolf, G.L., Shumacher, H.R. & Goldstein, E.J. (1985). Gadolinium oxide: A prototype agent for contrast enhanced imaging of the liver and spleen with magnetic resonance. *Magnetic Resonance Imaging* **3**, 65–71.

Bridot, J.-L., Faure, A.-C., Laurent, S., Riviere, C., Billotey, C., Hiba, B., Janier, M., Josserand, V., Coll, J.-L., Elst, L. V., Muller, R., Roux, S., Perriat, P. & Tillement, O. (2007). Hybrid gadolinium oxide nanoparticles: multimodal contrast agents for in vivo imaging. *Journal of the American Chemical Society* **129**, 5076-5084.

Bruchez, M., Moronne, M., Gin, P., Weiss, S., & Alivisatos A.P. (1998). Semiconductor nanocrystals as fluorescent biological labels. *Science* **281(5385)**, 2013–2016.

Cai, D., Mataraza, J.M., Qin, Z.H., Huang, Z., Huang, J., Chiles, T.C., Carnahan, D., Kempa, K. & Ren, Z., (2005). Highly efficient molecular delivery into mammalian cells using carbon nanotube spearing. *Nature Methods*, **2**, 449-454.

Cai, Q., Kim, S.H., Choi, K.S., Kim, S.Y., Byun, S. J., Kim, K.W., Park, S.H., Juhng, S.K. &Yoon, K.H. (2007a). Colloidal gold nanoparticles as a blood-pool contrast agent for X-ray computed tomography in mice. *Investigative Radiology* **42(12)**, 797-806.

Cai, W., Chen, K., Li, Z.B., Gambhir, S.S. & Chen, X. Y. (2007b). Dual-function probe for PET and near-infrared fluorescence imaging of tumor vasculature. *The Journal of Nuclear Medicine* **48**, 1862–1870.

Cai, W. & Chen, X.Y. (2007). Nanoplatforms for targeted molecular imaging in living subjects. *Small* **3**, 1840-1854.

Cai, W., Niu, G. & Chen, X.Y. (2007). Multimodality imaging of the HER-kinase axis in cancer. *European Journal of Nuclear Medicine and Molecular Imaging* DOI 10.1007/s00259-007-0560-9.

Cai, W., Shin, D. W., Chen, K., Gheysens, O., Cao, Q., Wang, S.X., Gambhir, S.S. & Chen, X. (2006). Peptide-labeled near-Infrared quantum dots for imaging tumor vasculature in living subjects. *Nano Letters* **6**, 669-676.

Cang, H., Sun, T., Li, Z.Y., Chen, J.Y., Wiley, B.J., Xia, Y.N. & Li, X.D. (2005). Gold nanocages as contrast agents for spectroscopic optical coherence tomography. *Optical Letters* **30(22)**, 3048-3050.

Carr, D.H., Brown, J., Bydder, G.M., Steiner, R.E., Weinmann, H.J., Speck, U., Hall, A.S. & Young, I.R. (1984). Gadolinium-DTPA as a contrast agent in MRI-initial clinical-experience in 20 patients. *American Journal of Roentgenology*, **143 (2)**, 215-224.

Chakrabarti, A., Zhang, K., Aruva, M. R., Cardi, C. A., Opitz, A. W., Wagner, N. J., Thakur, M. L. & Wiskstrom, E. (2007). Radio-hybridization PET Imaging of KRAS G12D mRNA expression in human pancreas cancer xenografts with [Cu-64]DO3A-Peptide nucleic acid-peptide nanoparticles. *Cancer Biology & Therapy* **6 (6)**, 948-956.

Chan, K.W.Y. & Wong, W.T. (2007). Small molecular gadolinium(III) complexes as MRI contrast agents for diagnostic imaging. *Coordination Chemistry Reviews* **251(17-20)**, 2428-2451.

Chan, W.C.W. & Nie S.M. (1998). Quantum dot bioconjugates for ultrasensitive nonisotopic detection. *Science* **281(5385)**, 2016–2018.

Chan, W.C.W., Maxwell, D.J., Gao X.H., Bailey, R.E., Han, M.Y. & Nie, S.M. (2002). Luminescent quantum dots for multiplexed biological detection and imaging. *Current Opinion in Biotechnology* **13**, 40–46.

Chapon, C., Franconi, F., Lemaire, L., Marescaux, L., Legras, P., Denizot, B. & Le Jeune, J.J. (2005). Volumetric assessment of myocardial viability in rats using 3D double contrast enhanced T1 and T2-weighted MRI. *Magnetic Resonance Materials in Physics, Biology and Medicine* **18 (6)**, 302-308.

Chavanpatil, M.D., Khdair, J. & Panyam, J. (2006). Nanoparticles for cellular drug delivery: mechanisms and factors influencing delivery. *Journal of Nanoscience and Nanotechnology* **6**, 2651-2663.

Chen, F.Q. & Gerion, D. (2004). Fluorescent CdSe/ZnS nanocrystal-peptide conjugates for long-term, nontoxic imaging and nuclear targeting in living cells. *Nano Letters* **4(10)**, 1827-1832.

Chen, J.Y., Wiley, B., Li, Z.Y., Campbell, D., Saeki, F., Cang, H., Au, L., Lee, J., Li, X.D. & Xia, Y.N. (2005). Gold nanocages: Engineering their structure for biomedical applications. *Advanced Materials* **17 (18)**, 2255-2261.

Chen, J.Y., Wang, D., Xi, J., Au, L., Siekkinen, A., Warsen, A., Li, Z.Y., Zhang, H., Xia, Y.N. & Li, X.D. (2007). Immuno gold nanocages with tailored optical properties for targeted photothermal destruction of cancer cells," Nano Letters 7(5), 1318-1322.

Cherukuri, P., Bachilo, S. M., Litovsky, S. H. & Weisman, R. B. (2004). Near-infrared fluorescence microscopy of single-walled carbon nanotubes in phagocytic cells. *Journal of the American Chemical Society* **126**, 15638 –15639.

Cherukuri, P., Gannon, C. J., Leeuw, T. K., Schmidt, H.K., Smalley, R.E., Curley, S.A., Weisman, R. B. (2006). Mammalian pharmacokinetics of carbon nanotubes using intrinsic near-infrared fluorescence. *Proceedings of the National Academy of Sciences of the United States of America* **103**, 18882-18886.

Choi, J.H., Nguyen, F.T., Barone, P.W., Heller, D.A., Moll, A.E., Patel, D., Boppart, S.A. & Strano, M.S. (2007). Multimodal biomedical imaging with asymmetric single-walled carbon nanotube/iron oxide nanoparticle complexes. *Nano Letters* **7(4)**, 861-867.

Chryssidis, .S, Davies, R.P. & Tie, M.L. (2002). Gadolinium-enhanced computed tomographic aortography. *Australasian Radiology* **46(1)**, 97–100.

Collier, T.L., Lecomte, R., McCarthy, T.J., Meikle, S., Ruth, T.J., Scopinaro, F., Signore, A., VanBrocklin, H., Van de Wiele C. & Waterhouse, R.N. (2002). Assessment of cancer-associated biomarkers by positron emission tomography: Advances and challenges. *Disease Markers* **18**, 211–247.

Corot, C. Robert, P., Idée, J.-M. & Port, M. (2006). Recent advances in iron oxide nanocrystal technology for medical imaging. *Advanced Drug Delivery Reviews* **58**, 1471–1504.

Coussios, C. C., Holland, C. K., Jakubowska, L., Huang, S. L., MacDonald, R. C., Nagaraj, A. & McPherson, D. D. (2004). In vitro characterization of liposomes and Optison by acoustic scattering at 3.5 MHz. Ultrasound in Medicine & Biology **30**, 181-190.

Cunningham, C.H., Arai, T., Yang, P.C., McConnell, M.V., Pauly, J.M. & Conolly, S.M. (2005). Positive contrast magnetic resonance imaging of cells and labeled with magnetic nanoparticles. *Magnetic Resonance in Medicine* **53**, 999-1005.

Dahan, M., Lévi, S., Luccardini, C., Rostaing, P., Riveau, B. &Triller, A. (2003). Diffusion dynamics of glycine receptors revealed by single-quantum dot tracking. *Science* **302**, 442-445.

de Geus-Oei, L.F., van der Heijden, H.F.M., Corstens, F.H.M. & Oyen, W.J.G. (2007). Predictive and prognostic value of FDG-PET in nonsmall-cell lung cancer. *Cancer* **110**, 1654-1664.

Dekker, C. (1999). Carbon nanotubes as molecular quantum wires. *Physics Today* **52(5)**, 22-28.

Demos, S.M., Alkan-Onyuksel, H., Kane, B.J., Ramani, K., Naqaraj, A., Greene, R., Kleqerman, M. & Mcpherson, D.D. (1999). *Journal of American College of Cardiology* **33**, 867-875.

Deng, T., Li, J.S., Jiang, J.H., Shen, G.L. & Yu, R.Q. (2006). Preparation of near-IR fluorescent nanoparticles for fluorescence-anisotropy-based immunoagglutination assay in whole blood. *Advanced Functional Materials* **16**, 2147-2155.

Derfus, A.M., Chan, W.C.W. & Bhatia, S.N. (2004a). Probing the cytotoxicity of semiconductor quantum dots. *Nano Letters* **4**, 11-18.

Derfus, A.M., Chan, W.C.W. & Bhatia, S.N. (2004b). Intracellular delivery of quantum dots for live cell labeling and organelle tracking. *Advanced Materials* **16(12)**, 961+.

Dunn, E.A., Weaver, L.C., Dekaban, G.A. & Foster P.J. (2005). Cellular imaging of inflammation after experimental spinal cord injury. *Molecular Imaging* **4**, 53-62.

Elliott, M.R. & Thrush, A.J. (1996). Measurement of resolution in intravascular ultrasound images. *Physiological Measurement* **17,** 259-265.

El-Sayed, I.H., Huang, X.H., El-Sayed, M.A. (2005). Surface plasmon resonance scattering and absorption of anti-EGFR antibody conjugated gold nanoparticles in cancer diagnostics: Applications in oral cancer. *Nano Letters* **5(5)**, 829-834.

El-Sayed, I.H., Huang, X.H., El-Sayed, M.A. (2006). Selective laser photo-thermal therapy of epithelial carcinoma using anti-EGFR antibody conjugated gold nanoparticles. *Cancer Letters* **239(1)**, 129-135.

Endres, P., Paunesku, T., Vogt, S., Meade, T. & Woloschak, G.E. (2007). DNA-TiO_2 nanoconjugates labeled with magnetic resonance contrast agents. *Journal of the American Chemical Society* **129(51)**, 15760-15761.

Enochs, W.S., Harsh, G., Hochberg, F. & Weissleder, R. (1999). Improved delineation of human brain tumors on MR images using a long-circulating, superparamagnetic iron oxide agent. *Journal Magnetic Resonance Imaging* **9**, 228-232.

Ekpo, M.D.; Xie, J.; Liu, X.; Onuku, R.; Boafo, G.F.; Tan, S. (2022) Incorporating cryopreservation evaluations into the design of cell-based drug delivery systems: An opinion paper. *Front Immunol.* **13**, 967731.

Farsiu, S., Christofferson, J., Eriksson, B., Milanfar, P., Friedlander, B., Shakouri, A. & Nowak, R. (2007). Statistical detection and imaging of objects hidden in turbid media using ballistic photons. *Applied Optics* **46(23)**, 5805-5822.

Fayad, Z.A., Nahar, T., Fallon, J.T., Goldman, M., Aguinaldo, J.G., Badimon, J.J., Shinnar, M., Chesebro, J.H. & Fuster, V. (2000). In vivo magnetic resonance evaluation of atherosclerotic plaques in the human thoracic aorta: a comparison with transesophageal echocardiography. *Circulation* **101**, 2503-2509.

Feinstein, S.B., Tencate, F.J., Zwehl, W., Ong, K., Maurer, G., Tei, C., Shah, P.M., Meerbaum, S. & Corday, E. (1984). Two-dimensional contrast echocardiography. 1. In vitro development and quantitative-analysis of echo contrast agents. *Journal of American College of Cardiology* **3**, 14–20.

Feinstein S.B., Cheirif, J., Tencate, F.J., Silverman, P.R., Heidenreich, P.A., Dick, C., Desir, R.M., Armstrong, W.F. Quinones, M.A. & Shah, P.M. (1990). Safety and efficacy of a new transpulmonary ultrasound contrast agent—initial multicenter clinical-results. *Journal of American College of Cardiology* **16**, 316–324.

Ferrara, K., Pollard, R. & Borden, M. (2007). Ultrasound microbubble contrast agents: fundamentals and application to gene and drug delivery. Annual Review of Biomedical Engineering **9**, 415–447.

Ferrucci, J.T. & Stark, D.D. (1990). Iron oxide-enhanced MR imaging of the liver and spleen: review of the first years. *American Journal of Roentgenology* **155**, 943-950.

Fortina, P., Kricka, L.J., Graves, D.J., Park, J., Hyslop, T., Tam, F., Halas, N., Surrey, S. & Waldman, S.A. (2007). Applications of nanoparticles to diagnostics and therapeutics in colorectal cancer. *Trends in Biotechnology* **24(4)**, 145-152.

Frenkel, P.A., Chen, S.Y., Thai, T., Shohet, R.V. & Grayburn, P.A. (2002). DNA-loaded albumin microbubbles enhance ultrasound-mediated transfection in vitro. *Ultrasound in Medicine & Biology* **28**, 817–822.

Frias, J.C., Williams, K.J., Fisher, E.A. & Fayad, Z.A. (2004). Recombinant HDL-like nanoparticles: a specific contrast agent for MRI of atherosclerotic plaques. *Journal of the American Chemical Society* **126**, 16316-16317.

Fritz, T. A., Unger, E. C., Sutherland, G. & Sahn, D. (1997). Phase I clinical trials of MRX-115. A new ultrasound contrast agent. *Investigative Radiology* **32**, 735-740.

Characterization and application of single fluorescent nanodiamonds as cellular biomarkers.

Fu, C.C., Lee, H.Y., Chen, K., Lim, T.S., Wu, H.Y., Lin, P.K., Wei, P.K., Tsao, P.H., Chang,H.C. & Fann, W. (2007). *Proceedings of the National Academy of Sciences of the United States of America* **104, 727-732.**

Fu, K., Sun, J., Bickford, L.R., Lin, A.W.H., Halas, N.J., Yu, T.K. & Drezek, R.A. (2008) Measurement of immunotargeted plasmonic nanoparticles' cellular binding: a key factor in optimizing diagnostic efficacy. *Nanotechnology* **19**, 045103(6pp).

Gao, X., Cui, Y., Levenson, R.M., Chung, L.W.K. & Nie, S. (2004). In vivo cancer targeting and imaging with semiconductor quantum dots. *Nature Biotechnology* **22**, 969-976.

Gazelle, G.S., Wolf, G.L., McIntire, G.L., Bacon, E.R., George, N., Halpern, E.F. & Toner, J.L. (1995). Hepatic imaging with iodinated nanoparticles: A comparison with iohexol in rabbits. *Academic Radiology* **2(8)**, 700 –704.

Gibson, A., Hebden, J., & Arridge, S. (2005). Recent advances in diffuse optical imaging. *Physics in Medicine and Biology* **50**, R1-R43.

Gobin, A.M., O'Neal, D.P., Watkins, D.M., Halas, N.J., Drezek, R.A., & West, J.L. (2005). Near infrared laser-tissue welding using nanoshells as an exogenous absorber. *Laser in Surgery and Medicine* **37(2)**, 123-129.

Goldman, E. R., Anderson, G.P., Tran, P.T., Mattoussi, H., Charles, P.T. & Mauro J.M. (2002a) Conjugation of luminescent quantum dots with antibodies using an engineered adaptor protein to provide new reagents for fluoroimmunoassays. *Analytical Chemistry* **274**, 841–847.

Goldman, E. R., Balighian E.D., Mattoussi, H., Kuno, M.K., Mauro, J.M., Tran, P.T. & Anderson, G.P. Avidin: A natural bridge for quantum dot-antibody conjugates. (2002b) *Journal of American Chemical Society* **122**, 6378–6382.

Gramiak, R. & Shah, P.M. (1968). Echocardiography of the aortic root. *Investigative Radiology* **3**, 356–366.

Grande, F.; Tucci, P. (2016) Titanium Dioxide Nanoparticles: a Risk for Human Health? *Mini Rev Med Chem* **16(9)**,762-769.

Grenier, N., Pedersen, M. & Hauger, O. (2006). Contrast agents for functional and cellular MRI of the kidney. *European Journal of Radiology* **60(3)**, 341-352.

Groves, A.M., Win, T., Haim, S.B. & Ell, P.J. (2007). Non-[^{18}F]FDG PET in clinical oncology. *Lancet Oncology* **8**, 822–830.

Hainfeld, J.F., Slatkin, D.N., Focella, T.M. & Smilowitz, H.M. (2006). Gold nanoparticles: a new X-ray contrast agent. *British Journal of Radiology* **79**, 248-253.

Hamilton, A.J., Huang, S.L., Warnick, D., Rabbat, M., Kane, B., Nagaraj, A., Klegerman, M. & McPherson, D.D. (2004). Intravascular ultrasound molecular imaging of atheroma components in vivo. *Journal of the American College of Cardiology* **43**, 453-460.

Harisinghani, M.G., Jhaveri, K.S., Weissleder, R., Schima, W., Saini, S., Hahn, P.F. & Mueller, P.R. (2001). MRI contrast agents for evaluating focal hepatic lesions. *Clinical Radiology* **56**, 714-725.

Harisinghani, M.G., Barentsz, J., Hahn, P.F., Deserno, W.M., Tabatabaei, S., van de Kaa, C.H., de la Rosette, J. & Weissleder, R. (2003). Noninvasive detection of clinically occult lymph-node metastases in prostate cancer. *The New England Journal of Medicine* **348**, 2491-2499.

He, X., Duan, J., Wang, K., Tan, W., Lin, X. & He, C. (2004). A novel fluorescent label based on organic dye-doped silica nanoparticles for HepG liver cancer cell recognition. *Journal of Nanoscience and Nanotechnology* **4**, 585-589.

Helft, G., Worthley, S.G., Fuster, V., Zaman, A.G., Schechter, C., Osende, J.I., Rodriquez, O.J., Fayad, Z.A., Fallon, J.T. & Badimon, J.J. (2001). Atherosclerotic aortic component qualification by noninvasive magnetic resonance imaging: an in vivo study in rabbits. *Journal of the American College of Cardiology* **37**, 1149-1154.

Hengerer, A., Wunder, A., Wagenaar, D.J., VIJA, A.H., Shah, M. & Grimm, J. (2005). From genomics to clinical molecular imaging. *Procceedings of the IEEE* **93(4)**, 819-828.

Henson, J.W., Nogueira, R.G., Covarrubias, D.J., Gonzalez, R.G. & Lev, M.H. (2004). Gadolinium-enhanced CT angiography of the circle of willis and neck. *American Journal of Neuroradiology* **25**, 969-972.

Hirsch, L.R., Stafford, R.J., Bankson, J.A., Sershen, S.R., Rivera, B., Price, R.E., Hazle, J.D., Halas, N.J. & West, J.L. (2003a) Nanoshell-mediated near-infrared thermal therapy of tumors under magnetic resonance guidance. *Proceedings of the National Academy of Sciences of the United States of America* **100(23)**, 13549-13554.

Hirsch, L.R., Jackson, J.B., Lee, A., Halas, N.J. & West, J. (2003b). A whole blood immunoassay using gold nanoshells. *Analytical Chemistry* **75(10)**, 2377-2381.

Hirsch, L.R., Halas, N.J. & West, J.L. (2005). Whole-blood immunoassay facilitated by gold nanoshell–conjugate antibodies. *Methods in Molecular Biology* **303**, 101–112, Humana Press.

Holschbach, M.H.& Olsson, R.A. (2002). Applications of adenosine receptor ligands in medical imaging by positron emission tomography. *Current Pharmaceutical Design* **8**, 2345-2352.

Horn, D. & Rieger, J. (2001). Organic nanoparticles in the aqueous phase-theory, experiment, and use. *Angewandte Chemie-International Edition in English* **40(23)**, 4331-4361.

Hoshino, A., Fujioka, K., Oku, T., Nakamura, S., Suga, M., Yamaguchi, Y., Suzuki, K., Yasuhara, M. & Yamamoto, K. (2004). Quantum dots targeted to the assigned organelle in living cells. *Microbiology and Immunology* **48**, 985–994.

Hoshino, A., Hanaki, K., Suzuki, K., & Yamamoto, K. (2004b). Applications of T-lymphoma labeled with fluorescent quantum dots to cell tracing markers in mouse body. *Biochemical and Biophysical Research Communications* **314(1)**, 46-53.

Houser, C. R. (1990). Cholinergic synapses in the central nervous system: Studies of the immunocytochemical localization of choline acetyltransferase. *Journal of Electron Microscopy Technique* **15**, 2-19.

Huang, S. L., Hamilton, A. J., Pozharski, E., Nagaraj, A., Klegerman, M. E., McPherson, D. D. & MacDonald, R. C. (2002). Physical correlates of the ultrasonic reflectivity of lipid dispersions suitable as diagnostic contrast agents. *Ultrasound in Medicine and Biology* **28**, 339-348.

Huang, H., Pierstorff, E., Osawa, E. & Ho, D. (2007). Active nanodiamond hydrogels for chemotherapeutic delivery. *Nano Letters* **7**, 3305-3314.

Huang, X.H., Jain, P.K., El-Sayed, I.H. & El-Sayed, M.A. (2006a). Determination of the minimum temperature required for selective photothermal destruction of cancer cells with the use of immunotargeted gold nanoparticles. *Photochemistry and Photobiology* **82(2)**, 412-417.

Huang, X., El-Sayed, I. H., Qian, W. & El-Sayed, M. A. (2006b). Cancer cell imaging and photothermal therapy in the near-Infrared region by using gold nanorods. *Journal of American Chemical Society* **128(6)**, 2115-2120.

Hyafil, F., Cornily, J-C., Feig, J.E., Gordon, R., Vucic, E., Amirbekian, V., Fisher, E.A., Fuster, V., L., Feldman, J. & Fayad, Z.A. (2007). Noninvasive detection of macrophages using a nanoparticulate contrast agent for computed tomography. *Nature Medicine* **13(5)**, 636-641.

Ido, T., Wan, C.N., Casella, J.S., Fowler, J.S., Wolf, A.P., Reivich, M. & Kuhl, D.E. (1978). Labeled 2-deoxy-D-glucose analogs: 18F labeled 2-deoxy-2-fluoro-D-glucose, 2-deoxy-2-fluoro-D-mannose and 14C-2-deoxy-2-fluoro-D-glucose. *Journal of Labeled Compounds& Radiopharmaceuticals* **14**, 175-183.

Iijima, S. (1991). Helical microtubules of graphitic carbon. *Nature* **354(6348)**, 56-58.

Iijima, S., & Ichihashi, T. (1993). Single-shell carbon nanotubes of 1-nm diameter. *Nature* **363(6430)**, 603-605.

Ito, M., Ogino, H., Oshima, H., Shiraki, N., Shibamoto, Y., Kasai, H., Mase, M., Kawamura, Y. & Miyati, T. (2006). Evaluation of CH3-DTPA-Gd (NMS60) as a new MR contrast agent: early phase II study in brain tumors and dual dynamic contrast-enhanced imaging. *Magnetic Resonance Imaging* **24(5)**, 625-630.

Jaffer, F.A., Nahrendorf, M., Sosnovik, D., Kelly, K.A., Aikaiva, E. & Weissleder, R. (2006). Cellular imaging of inflainination in atherosclerosis using magnetofluorescent nanomaterials. *Molecular Imaging* **5**, 85-92.

Jain, P. K., El-Sayed, I. H. & El-Sayed, M. A. (2007). Au nanoparticles target cancer. *Nano Today* **2**, 18-29.

Jaiswal, J.K., Mattoussi, H., Mauro, J.M. & Simon, S.M. (2002). Long-term multiple color imaging of live cells using quantum dot bioconjugates. *Nature Biotechnology* **21**, 47-51.

Jarkas, N., Votaw J.R., Voll, R.J., Williams, L., Camp, V.M., Owens, M.J., Purselle, D.C., Bremner, J.D., Kilts, C.D., Nemeroff, C.B. & Goodman, M.M. (2005). Carbon-11 HOMADAM: A novel PET radiotracer for imaging serotonin transporters. *Nuclear Medicine and Biology* **32(3)**, 211-224.

Jiang, Y.; Tian, B. (2018) Inorganic semiconductor biointerfaces. *Nature Reviews Materials* **3**, 473-490.

Kam, N. W. S., Jessop, T. C., Wender, P. A. & Dai, H. (2004). Nanotube molecular transporters: Internalization of carbon nanotube-protein conjugates into mammalian cells. *Journal of American Chemical Society*, **126**, 6850-6851.

Kam, N.W.S., O'Connell, M., Wisdom, J. A. & Dai, H. (2005). Carbon nanotubes as multifunctional biological transporters and near-infrared agents for selective cancer cell destruction. *Proceedings of the National Academy of Sciences of United States of America* **102**, 11600–11605.

Kam, N. W. S. & Dai, H. (2005). Carbon nanotubes as intracellular protein transporters: Generality and biological functionality. *Journal of American Chemical Society* **127**, 6021-6026.

Kam, N.W.S., Liu, Z. & Dai, H. (2005). Functionalization of carbon nanotubes via cleavable disulfide bonds for efficient intracellular delivery of siRNA and potent gene silencing. *Journal of American Chemical Society* **127(36)**, 12492 –12493.

Kannan, R., Rahing, V., Culter, C., Pandrapragada, R., Katti, K.K., Kattumuri, V., Robertson, J.D., Casteel, S.J., Jurisson, S., Smith, C., Boote, E. & Katti, K.V. (2006). Nanocompatible chemistry toward fabrication of targeted-specific gold nanoparticles. *Journal of American Chemical Society* **128**, 11342-11343.

Kao, C.Y., Hoffman, E.A., Beck, K.C., Bellamkonda, R.V. & Annapragada, A.V. (2003). Long-residence-time nano-scale liposomal iohexol for X-ray–based blood pool imaging. *Academic Radiology* **10(5)**, 475-483.

Kattumuri, V., Katti, K., Bhaskaran, S., Boote, E.J., Casteel, S.W., Fent, G.M., Robertson, D.J., Chandrasekhar, M., Kannan, R. & Katti, K.V. (2007). Gum-arabic as a phytochemical construct for the

stabilization of gold nanoparticles: In vivo pharmacokinetics and X-ray-contrast-imaging studies. *Small* **3(2)**, 333-341.

Kim, H. K., Kang S.J., Choi, S.K., Min, Y.H. & Yoon, C.S. (1999). Highly efficient organic/inorganic hybrid nonlinear optic materials via sol-gel process: Synthesis, optical properties, and photobleaching for channel waveguides. *Chemistry of Materials* **11**, 779-788.

Kim, S., Lim, Y.T., Soltesz, E.G., De Grand, A.M., Lee, J., Nakayama, A., Parker, J.A., Mihaljevic, T., Laurence, R.G., Dor, D.M. Cohn, L.H., Bawendi, M.G. & Franqioni, J.V. (2004.) Near-infrared fluorescent type II quantum dots for sentinel lymph node mapping. *Nature Biotechnology* **22**, 93-97.

Kim, S.H., Lee, J.M, Han, J.K., Lee, J.Y., Kang, W.J., Jang, J.Y., Shin, K.S., Cho, K.C. & Choi, B.I. (2006). MDCT and superparamagnetic iron oxide (SPIO)-enhanced MR findings of intrapancreatic accessory spleen in seven patients. *European Radiology* **16(9)**, 1887-1897.

Kim, D., Park, S., Lee, J. H., Jeong, Y.Y. & Jon, S. (2007). Antibiofouling polymer-coated gold nanoparticles as a contrast agent for in vivo X-ray computed tomography imaging. *Journal of American Chemical Society* **129(24)**, 7661-7665.

Kircher, M.F., Mahmood, U., King, R.S., Weissleder, R. & Josephson, L.A. (2003). Multimodal nanoparticle for preoperative magnetic resonance imaging and intraoperative optical brain tumor delineation. *Cancer Research* **63**, 8122–8125.

Klibanov, A.L. (1999).Targeted delivery of gas-filled microspheres, contrast agents for ultrasound imaging. *Advanced Drug Delivery Reviews* **37,** 139–57.

Klibanov, A. L., Rasche, P. T., Hughes, M. S., Wojdyla, J. K., Galen, K. P., Wible, J. H. Jr. & Brandenburger, G. H. (2002). Detection of individual microbubbles of an ultrasound contrast agent: fundamental and pulse inversion imaging. *Academic Radiology* **9**, Suppl 2, S279-S281.

Klibanov, A. L. (2005). Ligand-carrying gas-filled microbubbles: ultrasound contrast agents for targeted molecular imaging. *Bioconjugate Chemistry* **16**, 9-17.

Kobayashi, H., Kawamoto, S., Saga, T., Sato, N., Hiraga, A., Konishi, J., Togashi, K. & Brechbiel, M.W. (2001a). Micro-MR angiography of normal and intratumoral vessels in mice using dedicated intravascular MR contrast agents with high generation of polyamidoamine dendrimer core: reference to pharmacokinetic properties of dendrimer-based MR contrast agents. *Journal of Magnetic Resonance Imaging* **14**, 705–713.

Kobayashi, H., Saga, T., Kawamoto, S., Sato, N., Hiraga, A., Ishimori, T., Konishi, J., Togashi, K. & Brechbiel, M.W. (2001b). Dynamic micro-magnetic resonance imaging of liver micrometastasis in mice with a novel liver macromolecular magnetic resonance contrast agent DAB-Am64-(1B4M-Gd)(64), *Cancer Research* **61**, 4966-4970.

Kobayashi, H., Kawamoto, S., Jo, S., Sato, N., Saga, T., Hiraga, A., Konishi, J., Hu, S., Togashi, K., Brechbiel, M.W. & Star, R.A. (2002). Renal tubular damage detected by dynamic micro-MRI with a dendrimer-based MR contrast agent, *Kidney International* **61**, 1980–1985.

Kobayashi, H., Kawamoto, S., Star, R.A., Waldmann, T.A., Tagaya, Y. & Brechbiel, M.W. (2003). Micro-magnetic resonance lymphangiography in mice using a novel dendrimer-based magnetic resonance imaging contrast agent. *Cancer Research* **63**, 271-276.

Kobayashi, H., Reijnders, K., English, S., Yordanov, A.T., Milenic, D.E., Sowers, A.L., Citrin, D., Krishna, M.C., Waldmann, T.A., Mitchell, J.B. & Brechbiel, M.W. (2004a). Application of a macromolecular contrast agent for detection of alterations of tumor vessel permeability induced by radiation. *Clinical Cancer Research* **10**, 7712-7720.

Kobayashi, H., Jo, S., Kawamoto, S., Yasuda, H., Hu, X., Knopp, M.V., Brechbiel, M.W., Choyke, P.L. & Star, R.A. (2004b) Polyamine dendrimer-based MRI contrast agents for the functional kidney imaging to diagnose the acute renal failure. *Journal of Magnetic Resonance Imaging* **20**, 512– 518.

Kobayashi, H., Kawamoto, S., Sakai, Y., Choyke, P.L., Star, R.A., Brechbiel, M.W., Sato, N., Tagaya, Y., Morris, J.C. & Waldmann, T.A. (2004c). Lymphatic drainage imaging of breast cancer in mice by micro-magnetic resonance lymphangiography using a nano-size paramagnetic contrast agent. *Journal of National Cancer Institute* **96**, 703-708.

Kobayashi, H. & Brechbiel M.W. (2005). Nano-sized MRI contrast agents with dendrimer cores. *Advanced Drug Delivery Reviews* **57**, 2271-2286.

Kobayashi, H., Kawamoto, S., Bernardo, M., Brechbiel, M.W., Knopp, M. V. & Choyke, P. L. (2006). Delivery of gadolinium-labeled nanoparticles to the sentinel lymph node: Comparison of the sentinel node visualization and estimations of intra-nodal gadolinium concentration by the magnetic resonance imaging. *Journal of Controlled Release* **111 (3)**, 343-351.

Kooi, M.E., Cappendijk, V.C., Cleutjens, K.B., Kessels, A.G., Kitslaar, P.J., Borgers, M., Frederik, P.M., Daemen, M.J. & van Engelshoven, J.M. (2003). Accumulation of ultrasmall superparamagnetic particles of iron oxide in human atherosclerotic plaques can be detected by in vivo magnetic resonance imaging. *Circulation* **107**, 2453-2458.

Korpanty, G., Grayburn, P.A., Shohet, R.V. & Brekken, R.A. (2005). Targeting vascular endothelium with avidin microbubbles. *Ultrasound in Medicine and Biology* **31**, 1279-1283.

Kruger Hagen, E., Forsberg, F., Aksnes, A.-K., Merton, D. A., Liu, J., Tornes, A., Johnson, D. & Goldberg, B. B. (2000) Enhanced detection of blood flow in the normal canine prostate using an ultrasound contrast agent-original investigations. *Investigative Radiology* **35(2)**, 118-124.

Långström, B., Itsenko, O. & Rahman, O. (2007). [11C] Carbon monoxide, a versatile and useful precursor in labelling chemistry for PET-ligand developmenty. *Journal of Labeled Compounds& Radiopharmaceuticals* **50**, 794–810.

Lanza, G. M., Wallace, K. D., Scott, M. J., Cacheris, W. P., Abendschein, D. R., Christy, D. H., Sharkey, A. M., Miller, J. G., Gaffney, P. J. & Wickline, S. A. (1996). A novel site targeted ultrasonic contrast agent with broad biomedical application. *Circulation* **94**, 3334-3340.

Lanza, G.M.,Wallace, K.D., Fischer, S.E., Christy, D.H., Scott, M.J., Trousil, R.L., Cacheris, W.P., Miller, J.G., Gaffney, P.J. & Wickline, S.A.(1997). High frequency ultrasonic detection of thrombi with a targeted contrast system. *Ultrasound in Medicine and Biology* **23**, 863–70.

Lauffer, R.B., Greif, W.L., Stark, D.D., Vincent, A.C., Saini, S., Wedden, V.J. & Brady T.J. (1985). Iron-EHPG as a hepatobiliary MR contrast agent-initial imaging and biodistribution studies. *Journal of Computer Assisted Tomography* **9(3)**, 431-438.

Laurent, S., Vander Elst, L. & Muller, R.N. (2006) Comparative study of the physicochemical properties of six clinical low molecular weight gadolinium contrast agents. *Contrast Media and Molecular Imaging* **1(3)**, 128-137.

Lee, K.J., Nallathamby, P.D., Browning, L.M., Osgood, C.J. & Xu, X.H.N. (2007a). In vivo imaging of transport and biocompatibility of single silver nanoparticles in early development of zebrafish embryos. *ACS Nano* **1(2)**, 133-143.

Lee, J., Burdette, J.E., MacRenaris, K.W., Mustafi, D., Woodruff, T. K. & Meade T.J. (2007b). Rational design, synthesis, and biological evaluation of progesterone-modified MRI contrast agents. *Chemistry & Biology* **14(7)**, 824 -834.

Lee, J., Huh, Y., Jun, Y., Seo, J., Jang, J., Song, H., Kim, S., Cho, E., Yoon, H., Suh, J. & Cheon, J. (2007c) Artificially engineered magnetic nanoparticles for ultra-sensitive molecular imaging. *Nature Medicine* **13**, 95-99.

Leeuw, T.K., Reith, R.M., Simonette, R.A., Harden, M.E., Cherukuri, P., Tsyboulski, D.A., Beckingham, K.M. & Weisman, R.B. (2007). Single-walled carbon nanotubes in the intact organism: Near-IR imaging and biocompatibility studies in Drosophila. *Nano Letters* **7(9)**, 2650 –2654.

Leighton, T. G. (1997). The acoustic bubble, Academic Press, London.

Lentacker, I., De Geest, B.G., Vandenbroucke, R.E., Peeters, L., Demeester, J., De Smedt, S.C. & Sanders, N.N. (2006). Ultrasound-responsive polymer-coated microbubbles that bind and protect DNA. *Langmuir* **22**, 7273–7278.

Leong-Poi, H., Christiansen, J., Klibanov, A.L., Kaul, S. & Lindner, J.R. (2003). Noninvasive assessment of angiogenesis by ultrasound and microbubbles targeted to alpha(v)-integrins. *Circulation* **107**, 455-460.

Levy, G. C., Dechter, J. J., & Kowalewski, J. (1978). The effect of paramagnetic relaxation reagents on nitrogen-15 spin relaxation and the use of Gd(dpm)3 as a nitrogen-15 nuclear magnetic resonance spin label. *Journal of American Chemical Society* **100**, 2308-2314.

Lewin, M., Carlesso, N., Tung, C.H., Tang, X.W., Cory, D., Scadden, D.T. & Weissleder, R. (2000). Tat Peptide-derivatized magnetic nanoparticles allow in vivo tracking and recovery of progenitor cells. *Nature Biotehcnology* **18**, 410-414.

Li, L.; Yang, J.; Wei, J.; Jiang,C.; Liu, Z.; Yang, B.; Zhao, B.; Song, W. (2022) SERS monitoring of photoinduced-enhanced oxidative stress amplifier on Au@carbon dots for tumor catalytic therapy, *Light: Science & Applications* **11**, Article number: 286.

Lidke, D.S., Nagy, P., Heintzmann, R., Arndt-Jovin, D.J., Post, J.N., Grecco, H.E., Jares-Erijman, E.A. & Jovin, T.M. (2004). Quantum dot ligands provide new insights into erbB/HER receptormediated signal transduction. *Nature Biotechnology* **22**, 198–203.

Lindner, J.R., Song, J., Christiansen, J., Klibanov, A.L., Xu, F. & Ley, K. (2001). Ultrasound assessment of inflammation and renal tissue injury with microbubbles targeted to P-selectin. *Circulation* **104**, 2107-2112.

Lipinski, M.J., Amirbekian, V., Frais, J.C., Aguinaldo, J.G., Mani, V, Briley-Saebo, K.C., Fuster, V., Fallon, J.T., Fischer, E.A. & Fayad, Z.A. (2006). MRI to detect atherosclerosis with gadolinium-containing immunomicelles targeting the macrophage scavenger receptor. *Magnetic Resonance in Medicine* **56**, 601-610.

Lisy, M.R., Hartung, A., Lang, C., Schüler, D., Richter, W., Reichenbach, J.R., Kaiser, W.A. & Hilger, I. (2007). Fluorescent bacterial magnetic nanoparticles as bimodal contrast agents. *Investigative Radiology* **42**, 235–241.

Liu, Y., Wu, D. C., Zhang, W.D., Jiang, X., He, C. B., Chung, T. S., Goh, S. H. & Leong, K. W. (2005). Polyethylenimine-grafted multiwalled carbon nanotubes for secure noncovalent immobilization and efficient delivery of DNA. *Angewandte Chemie International Edition in English* **44**, 4782-4785.

Liu, J., Levine, A. L., Mattoon, J. S., Yamaguchi, M., Lee, R. J., Pan, X. & Rosol, T. J. (2006). Nanoparticles as image enhancing agents for ultrasonography. *Physics in Medicine and Biology* **51**, 2179–2189.

Liu, J., Li, J., Rosol, T. J., Pan, X. & Voorhees, J. L. (2007a). Biodegradable nanoparticles for targeted ultrasound imaging of breast cancer cells in vitro. *Physics in Medicine and Biology* **52**, 4739–4747.

Liu, Z., Cai, W., He, L., Nakayama, N., Chen, K., Sun, X.M., Chen, X.Y. & Dai, H.J. (2007b). In vivo biodistribution and highly efficient tumour targeting of carbon nanotubes in mice. *Nature Nanotechnology* **2**, 47-52.

Loo, C., Lin, A., Hirsch, L., Lee, M.H., Barton, J., Halas, N., West, J. & Drezek, R. (2004). Nanoshell-enabled photonics-based imaging and therapy of cancer. *Technology in Cancer Research & Treatment* **3 (1)**, 33-40.

Loo, C., Lowery, A., Halas, N., West, J. & Drezek, R. (2005a). Immunotargeted nanoshells for integrated cancer imaging and therapy. *Nano Letters* **5(4)**, 709-711.

Loo, C., Hirsch, L., Lee, M.H., Chang, E., West, J., Halas, N. & Drezek, R. (2005b). Gold nanoshell bioconjugates for molecular imaging in living cells. *Optical Letters* **30(9)**, 1012-1014.

Lu, Q., Moore, J. M., Huang, G., Mount, A. S., Rao, A. M., Larcom, L. L. & Ke, P. C. (2004). RNA polymer translocation with single-walled carbon nanotubes. *Nano Letters*, **4**, 2473-2477.

Machtens, S., Serth, J., Meyer, A., Kleinhorst, C., Ommer, K.J., Herbst, U., Kieruij, M.& Boerner, A.R. (2007). Positron emission tomography (PET) in the urooncological evaluation of the small pelvis. *World Journal of Urology* **25**, 341–349.

Mahtab, R., Harden, H. H. & Murphy, C.J. (2000). Temperature- and salt-dependent binding of long protein-sized quantum dots: thermodynamics of "inorganic protein"-DNA interactions. *Journal of American Chemical Society* 122, 14-17.

Makalowski, W. (2001). The human genome structure and organization. *Acta Biochimica Polonica* **48**, 587-598.

Mani, V., Briley-Saebo, K.C., Itskovich V.V., Samber, D.D. & Fayad, Z.A. (2006). Gradient echo acquisition for superparamagnetic particles with positive contrast (GRASP): sequence characterization in

membrane and glass superparamagnetic iron oxide phantoms at 1.5 T and 3T. *Magnetic Resonance in Medicine* **55**, 126-135.

Manikandan, N.; Suresh Kumar, V.P.; Siva Murugan, S.; Rathis, G.; Vishnu Saran, K.; Shabariganesh, T.K. (2021) Carbon nanotubes and their properties. *Materials Today: Proceedings*, **47(14)**, 4682-4685，

Mankoff, D.A. & Eubank, W.B. (2006). Current and future use of positron emission tomography (PET) in breast cancer. *Journal of Mammary Gland Biology and Neoplasia* **11,** 125–136.

Massoud, T.F. & Gambhir, S.S. (2003). Molecular imaging in living subjects: seeing fundamental biological processes in a new light. *Genes & Development* **17**, 545-580.

Mcintire, G.L., Bacon, E.R., Illig, K.J., Coffey, S.B., Singh, B., BESSIN, G., Shore, M.T., Wolf, G.L. (2000). Time course of nodal enhancement with CT X-ray nanoparticle contrast agents: Effect of particle size and chemical structure. *Investigative Radiology* **35**, 91-96.

Mendonca-Dias, M.H., Gaggelli, E. & Lauterbur, P.C. (1983). Paramagnetic contrast agents in nuclear magnetic-resonance medical imaging. *Seminars in Nuclear Medicine* **13(4)**, 364-376.

Mendoca-Dias, M.H. & Lauterbur, P.C. (1986). Ferromagnetic particles as contrast agents for magnetic resonance imaging of the liver and spleen. *Magnetic Resonance in Medicine* **3**, 328-330.

Meza, M., Greener, Y., Hunt, R., Perry, B., Revall, S., Barbee, W., Murgo, J, P. & Cheirif, J. (1996). Myocardial contrast echocardiography: reliable, safe, and efficacious myocardial perfusion assessment after intravenous injections of a new echocardiographic contrast agent. *American Heart Journal* **132**, 871-881.

Michalet, X., Pinaud, F.F., Bentolila, L.A., Tsay, J.M., Doose, S., Li, J.J., Sundaresan, G., Wu, A.M., Gambhir, S.S. & Weiss, S. (2005). Quantum dots for live cells, in vivo imaging, and diagnostics. *Science* **307**, 538–544.

Mie, G. (1908). Beiträge zur Optik trüber Medien, speziell kolloidaler Metallösungen. *Annalen der Physik (Leipzig)* **330**, 377–445.

Miyamoto, A., Okimoto, H., Shinohara, H. & Shibamoto, Y., (2006). Development of water-soluble metallofullerenes as X-ray contrast media. *European Radiology* **16**, 1050-1053.

Mukundan, S. Jr., Ghaghada, K.B., Badea, C.T., Kao, C.Y., Hedlund, L.W., Provenzale, J.M., Johnson, G.A., Chen, E., Bellamkonda, R.V. & Annapragada, A. (2006). A liposomal nanoscale contrast agent for preclinical CT in mice. *American Journal of Roentgenology* **186(2)**, 300-307.

Mulder, W.J.M., Douma, K., Koning, G.A., Van Zandvoort, M.A., Lutgens, E., Daemen, M.J., Nicolay, K. & Strijkers, G.J. (2006). Liposome-enhanced MRI of neointimal lesions in the ApoE-KO mouse. *Magnetic. Resonance in Medicine* **55(5)**, 1170-1174.

Mulder, W.J.M., Griffioen, A.W., Strijkers, G.J., Cormode, D.P., Nicolay, K. & Fayad, Z.A. (2007). Magnetic and fluorescent nanoparticles for multimodality imaging. *Nanomedicine* **2**, 307-324.

Murakami, T., Ajima, K., Miyawaki, J., Yudasaka, M., Iijima, S. & Shibe, K. (2004). Drug-loaded carbon nanohorns: adsorption and release of dexamethasone in vitro. *Molecular Pharmaceutics*, **1**, 399-405.

Narayan, R.J., Wei, W., Jin, C., Andara, M., Agarwal, A., Gerhardt, R.A., Shih, C.C., Shih, C.M., Lin, S.J., Sun, Y.Y. & Ramamurti, R. (2006). Microstructural and biological properties of nanocrystalline diamond coatings. *Diamond and Related Materials* **15**, 1935-1940.

Neuwelt E.A., Várallyay, P., Bagó, A.G., Muldoon, L.L., Nesbit, G. & Nixon, R. (2004). Imaging of iron oxide nanoparticles by MR and light microscopy in patients with malignant brain tumors. *Neuropathology and Applied Neurobiology* **30**, 456–471.

Nie, S.M., Xing, Y., Kim, G.J. & Simons, J.W. (2007). Nanotechnology applications in cancer. *Annual Review of Biomedical Engineering* **9**, 257-288.

Nolte, I., Vince, G. H., Maurer, M., Herbold, C., Goldbrunner, R., Solymosi, L., Stoll, G. & Bendszus, M. (2005). Iron particles enhance visualization of experimental gliomas with high-resolution sonography. *American Journal of Neuroradiology* **26**, 1469–1474.

Nutt, R. (2007). The history of positron emission tomography (PET). *Molecular Imaging and Biology* **4**, 11-26.

O'Neal, D.P., Hirsch, L.R., Halas, N.J., Payne, J.D. & West, J.L. (2004). Photo-thermal tumor ablation in mice using near infrared-absorbing nanoparticles. *Cancer Letters* **209(2)**, 171-176.

Ornes， S. (2016). Quantum dots. *Proceedings of the National Academy of Sciences of the United States of America* **113(11)**, 2796-2797.

Pantarotto, D., Partidos, C.D., Graff, R., Hoebeke, J., Briand, J.P., Prato, M. & Bianco, A. (2003). Synthesis, structural characterization, and immunological properties of carbon nanotubes functionalized with peptides. *Journal of American Chemical Society* **125**, 6160–6164.

Pantarotto, D., Briand, J., Prato, M. & Bianco, A. (2004a). Translocation of bioactive peptides across cell membranes by carbon nanotubes. *Chemical Communications* **(1)**, 16-17.

Pantarotto, D., Singh, R., McCarthy, D., Erhardt, M., Briand, J.P., Prato, M., Kostarelos, K. & Bianco, A. (2004b). Functionalized carbon nanotubes for plasmid DNA gene delivery. *Angewandte Chemie International Edition in English* **43**, 5242–5246.

Parak, W.J., Boudreau, R., Le Gros, M., Gerion, D., Zanchet, D., Micheel, C.M., Williams, S.C., Alivisatos, A.P., Larabell, C. (2002). Cell motility and metastatic potential studies based on quantum dot imaging of phagokinetic tracks. *Advanced Materials* **14 (12)**, 882-885.

Patton, D. (1994) Roentgen and the new light-Roentgen's moment. Part 4: Of gastrointestinal radiology, bread and butter; or the flowering of barium sulfate. *Investigative Radiology* **29 (4)**, 472-479.

Paunesku, T., Rajh, T., Wiederrecht, G., Maser, J., Vogt, S., Stojicevic, N., Protic, M., Lai, B., Oryhon, J., Thurnauer, M. & Woloschak, G. (2003). Biology of TiO_2-oligonucleotide nanocomposites. *Nature Materials* **2(5)**, 343-346.

Paunesku, T., Vogt, S., Maser, J., Lai, B. & Woloschak, G. (2006). X-ray fluorescence microprobe imaging in biology and medicine. J. Cellular Biochemistry **99(6)**, 1489-1502.

Paunesku, T., Vogt, S., Lai, B., Maser, J., Stojicevic, N., Thurn, K.T., Osipo, C., Liu, H., Legnini, D., Wang, Z., Lee, C. & Woloschak, G.E. (2007). Intracellular distribution of TiO_2-DNA oligonucleotide nanoconjugates directed to nucleolus and mitochondria indicates sequence specificity**.** *Nano Letters* **7(3)**, 596-601.

Porter, A.E., Gass, M., Muller, K., Skepper, J.N., Midgley, P.A. & Welland, M. (2007). Direct imaging of single-walled carbon nanotubes in cells. *Nature Nanotechnology* **2**, 713-717.

Pressly, E.D., Rossin, R., Hagooly, A., Fukukawa, K., Messmore, B.W., Welch, M.J., Wooley, K.L., Lamm, M. S., Hule, R.A., Pochan, D.J. & Hawker, C.J. (2007). Structural effects on the biodistribution and positron emission tomography (PET) imaging of well-defined ^{64}Cu-labeled nanoparticles comprised of amphiphilic block graft copolymers. *Biomacromolecules* **8**, 3126-3134.

Quinn, A.D., O'Hare, N.J., Wallis, F.J. & Wilson, G.F. (1994). Gd-DTPA: an alternative contrast medium for CT. *Journal of Computer Assisted Tomography* **18**, 634–636.

Rabin, O., Perez, M., Grimm, J., Wojtkiewicz, G. & Weissleder, R. (2006). An X-ray computed tomography imaging agent based on long-circulating bismuth sulphide nanoparticles. *Nature Materials* **5**, 118-122.

Räty, J.K., Liimatainen, T., Kaikkonen, M.U., Gröhn, O., Airenne, K. J. & Ylä-Herttuala, S. (2007). Non-invasive imaging in gene therapy. *Molecular Therapy* **15(9)**, 1579–1586.

Roeda, D., Kuhnasti, B., Hammadi, A. & Dollé, F. (2007). The service hospitalier Frédéric Joliot – contributions to PET-chemistry over the years. *Journal of Labelled Compounds and Radiopharmaceuticals* **50**, 848–866.

Rosenthal, S.J., Tomlinson, I., Adkins, E.M., Schroeter, S., Adams, S., Swafford, L., McBride, J., Wang, Y., DeFelice, L.J. & Blakely, R.D. (2002). Targeting cell surface receptors with ligand-conjugated nanocrystals. *Journal of American Chemical Society* 124, 4586-4594.

Saini, S., Stark, D.D., Hahn, P.F., Wittenberg, J. Brady T.J. & Ferrucci, J.T. (1987). Ferrite particles-a superparamagnetic MR contrast agent for the reticuloendothelial system. *Radiology* **162(1)**, 211-216.

Sakamoto, J.H., Smith, B.R., Xie, B., Rokhlin, S.I., Lee, S.C. & Ferrari, M. (2005). The molecular analysis of breast cancer utilizing targeted nanoparticle based ultrasound contrast agents. *Technology in Cancer Research and Treatment* **4(6)**, 627-636.

Santra, S., Zhang, P., Wang, K.M., Tapec, R. & Tan, W.H. (2001). Conjugation of biomolecules with luminophore-doped silica nanoparticles for photostable biomarkers. *Analytical Chemistry* **73**, 4988-4993.

Santra, S., Liesenfeld, B., Dutta, D., Chatel, D., Batich, C.D., Tan, W.H., Moudgil, B.M. & Mericle, R.A. (2005). Folate conjugated fluorescent silica nanoparticles for labeling neoplastic cells. *Journal of Nanoscience and Nanotechnology* **5**, 899-904.

Schmidt, G. & Malwitz, M.M. (2003). Properties of polymer-nanoparticle composites. *Current Opinion in Colloid & Interface Science* **8(1)**, 103-108.

Schulze, E., Ferrucci, J.T. Jr, Poss, K., Lapointe, L., Bogdanova, A. & Weissleder, R. (1995) Cellular uptake and trafficking of a prototypical magnetic iron oxide label in vitro. *Investigative Radiology* **30**, 604-610.

Seo , J., Chung , H., Kim ,M., Lee , J., Choi, I. & Cheon, J. (2007). Development of water-soluble single-crystalline TiO_2 nanoparticles for photocatalytic cancer-cell treatment. *Small* **3**, 850–853.

Seo, W., Lee, J., Sun, X., Suzuki, Y., Mann, D., Liu, Z., Terashima, M., Yang, P. C., McConnell, M.V., Nishimura, D. G. & Dai, H. (2006). FeCo/graphitic-shell nanocrystals as advanced magnetic-resonance-imaging and near-infrared agents. *Nature Materials* **5(12)**, 971-976.

Simonsen, C.Z., Ostergaard, L., Vestergaard-Poulsen, P., Rohl, L., Bjornerud, A. & Gyldensted, C. (1999). CBF and CBV measurements by USPIO bolus tracking: reproducibility and comparison with Gd-based values. *Journal of Magnetic Resonance Imaging* **9**, 342-347.

Singh, R., Pantarotto, D., McCarthy, D., Chaloin, O., Hoebeke, J., Partidos, C.D., Briand, JP, Prato, M, Bianco, A. & Kostarelos, K. (2005). Binding and condensation of plasmid DNA onto functionalized carbon nanotubes: Toward the construction of nanotube-based gene delivery vectors. *Journal of American Chemical Society*, **127**, 4388–4396.

Singh, R., Pantarotto, D., Lacerda, L., Pastorin, G., Klumpp, C., Prato, M., Bianco, A. & Kostarelos, K., (2006). Tissue biodistribution and blood clearance rates of intravenously administered carbon nanotube radiotracers. *Proceedings of the National Academy of Sciences of United States of America* **103**, 3357–3362.

Sipkins, D.A., Cheresh, D.A., Kazemi, M.R., Nevin, L.M., Bednarski, M.D. & Li, K.C. (1998). Detection of tumor angiogenesis in vivo by alpha(v)beta(3)-targeted magnetic resonance imaging. *Nature Medicine* **4**, 623-626.

Skinner, M.P., Yuan, C., Mitsumori, L., Hayes, C.E, Raines, E.W., Nelson, J.A. & Ross, R. (1995). Serial magnetic resonance imaging of experimental atherosclerosis detects lesion fine structure, progression and complications in vivo. *Nature Medicine* **1**, 69-73.

Smith, J. E., Wang, L. & Tan, W.H. (2006). Bioconjugated silica-coated nanoparticles for bioseparation and bioanalysis. *TRAC-Trends in Analytical Chemistry* **25**, 848-855.

Sokolov, K., Follen, M., Aaron, J., Pavlova, I., Malpica, A., Lotan, R. & Richards-Kortum, R. (2003). Real time vital imaging of pre-cancer using anti-EGFR antibodies conjugated to gold nanoparticles. *Cancer Research* **63**, 1999-2004.

Song, J., Qi, M., Kaul, S. & Price, R. J. (2002). Stimulation of arteriogenesis in skeletal muscle by microbubble destruction with ultrasound. *Circulation* **106**, 1550-1555.

Stark, D.D., Weissleder, R., Elizondo, G., Hahn, P.F., Saini, S., Todd, L.E., Wittenberg, J. & Ferrucci, J.T. (1988). Superparamagnetic iron-oxide-clinical applications as a contrast agent for MR imaging of the liver. *Radiology* **168(2)**, 297-301.

Stell, A., Belcredito, S., Ramachandran, B., Biserni, A., Rando, G., Ciana, P. & Maggi, A. (2007). Multimodality imaging: novel pharmacological applications of reporter systems. *Quarterly Journal of Nuclear Medicine and Molecular Imaging* **51**, 127-138.

Suga, K., Yuan, Y., Ueda, K., Kaneda, Y., Kawakami, Y., Zaki, M. & Matsunaga, N. (2004). Computed tomography lymphography with intrapulmonary injection of lopamidol for sentinel lymph node localization. *Investigative Radiology* **39(6)**, 313-324.

Sun, G., Xu, J., Hagooly, A., Rossin, R., Li, Z., Moore, D.A., Hawker, C.J., Welch, M.J. & Wooley, K.L. (2007). Strategies for optimized radiolabeling of nanoparticles for in vivo PET imaging. *Advanced Materials* **19**, 3157–3162.

Talanov, V.S., Regino, C.A.S., Kobayashi, H., Bernardo, M., Choyke, P.L. & Brechbiel, M.W. (2006). Dendrimer-based nanoprobe for dual modality magnetic resonance and fluorescence imaging. *Nano Letters* **6**, 1459-1463.

Tan, W.H., Wang, K.M., He, X.X., Zhao, X.J., Drake, T., Wang, L. & Bagwe, R.P. (2004a) Bionanotechnology based on silica nanoparticles. *Medicinal Research Reviews* **24**, 621-638.

Tan, M., Wang, G., Hai, X., Ye, Z. & Yuan, J. (2004b). Developemnt of functionalized fluorescent europium nanoparticles for biolabeling and time-resolved fluorometric applications. *Journal of Materials Chemistry* **14**, 2896-2901.

Tesauro, D., Accardo, A., Gianolio, E., Paduano, L., Teixeira, J., Schillén, K., Aime, S. & Morelli, G. (2007). Peptide derivatized lamellar aggregates as target-specific MRI contrast agents. *Chembiochem* **8(8)**, 950-955.

Thomsen, H.S. & Morcos, S.K. (2000). Radiographic contrast media. *British Journal of Urology International* **86(s1)**, 1-10.

Thurn, K.T., Brown, E.M.B., Wu, A., Vogt, S., Lai, B., Maser, J., Paunesku, T. & Woloschak, G.E. (2007) Nanoparticles for applications in cellular imaging. *Nanoscale Research Letters* **2**, 430–441.

Tong, R. & Cheng J.J. (2007). Anticancer polymeric nanomedicines. *Polymer Reviews* **47 (3)**, 345-381.

Toussaint, J.F., LaMuraglia, G.M., Southern, J.F., Fuster, V. & Kantor, H.L. (1996). Magnetic resonance images lipids, fibrous, calcified, hemorrhagic, and thrombotic components of human atheroscerosis in vivo. *Circulation* 94, 932-938.

Turvey, S.E., Swart, E., Denis, M.C., Mahmood, U., Benoist, C., Weissleder, R. & Mathis, D. (2005). Noninvasive imaging of pancreatic inflammation and its reversal in type 1 diabetes. *Journal of Clinical Investigation* **115**, 2454-2461.

Vallabhajosula, S. (2007). ^{18}F-Labeled positron emission tomographic radiopharmaceuticals in oncology: an overview of radiochemistry and mechanisms of tumor localization. *Seminars in Nuclear Medicine* **37**, 400-419.

van Tilborg, G.A.F., Mulder, W.J.M., Deckers, N., Storm, G., Reutelingsperger, C.P.M., Strijkers, G.J. & Nicolay, K. (2006). Annexin A5-functionalized bimodal lipid-based contrast agents for the detection of apoptosis. *Bioconjugate Chemistry* **17**, 741-749.

Veiseh, O., Sun, C., Gunn, J., Kohler, N., Gabikian, P., Lee, D., Bhattarai, N., Ellenbogen, R., Sze, R., Hallahan, A., Olson, J. & Zhang, M. (2005). Optical and MRI multifunctional nanoprobe for targeting gliomas. *Nano Letters* **5**, 1003–1008.

Vosch, T., Antoku, Y., Hsiang, J.C., Richards, C.I., Gonzalez, J.I. & Dickson, R.M. (2007). Strongly emissive individual DNA-encapsulated Ag nanoclusters as single-molecule fluorophores. *Proceedings of the National Academy of Sciences of the United States of America* 104, 12616-12621.

Wang, H.F., Wang, J., Deng, X.Y., Sun, H.F., Shi, Z.J., Gu, Z.N., Liu, Y.F. & Zhao, Y.L. (2004). Biodistribution of carbon single-wall carbon nanotubes in mice. *Journal of Nanoscience and Nanotechnology*, **4**, 1019–1024.

Wang, H., Huff, T.B., Zweifel, D.A., He, W., Low, P.S., Wei, A. & Cheng, J. (2005). In vitro and in vivo two-photon luminescence imaging of single gold nanorods. *Proceedings of the National Academy of Sciences of the United States of America* **102**, 15752-15756.

Wang, J.; Chen, Y.; Wang, S.; Liu, H.; Zhao, F. (2021) Investigations on the Influencing Mechanisms of SiO_2 Nanoparticles on Foam Stability. *Energy Fuels* **35(24)** 20016-20025.

Wang, L., Yang, C.Y. & Tan, W.H. (2005). Dual-luminophore-doped silica nanoparticles for multiplexed signaling. *Nano Letters* **5**, 37-43.

Wang, L. & Tan, W. (2006). Multicolor FRET silica nanoparticles by single wavelength excitation. *Nano Lett.* **6(1)**, 84-88.

Wang, Y.X., Hussain, S.M. & Krestin, G.P. (2001). Superparamagnetic iron oxide contrast agents: physicochemical characteristics and applications in MR imaging. *European Radiology* **11**, 2319-2331.

Wang, Y.; Zhang, H.; Wang, Z.; Feng, L. (2020). Photothermal Conjugated Polymers and Their Biological Applications in Imaging and Therapy. *ACS Appl. Polym. Mater.* **2(10)**, 4222-4240.

Warmuth, C., Schnorr, J., Kaufels, N., Wagner, S., Pilgrimm, H., Hamm, B. & Taupitz, M. (2007). Whole-heart coronary magnetic resonance angiography-Contrast-enhanced high-resolution, time-resolved 3D imaging. *Investigative Radiology* **42(8)**, 550-557.

Watkin, K.L. & McDonald, M.A. (2002). Multi-modal contrast agents: A first step. *Academic Radiology* **9(suppl 2)**, S285–S289.

Weissleder, R., Elizondo, G., Wittenberg, J., Rabito, C.A., Bengele, H.H. & Josephson, L. (1990a). Ultrasmall superparamagnetic iron oxide: characterization of a new class of contrast agents for MR imaging. *Radiology* **175**, 489-493.

Weissleder, R., Lee, A.S., Fischman, A.J., Reimer, P., Shen, T., Wilkinson, R., Callahan, R.J. & Brady, T.J. (1990b) Ultrasmall superparamagnetic iron oxide: an intravenous contrast agent for assessing lymph nodes with MR imaging. *Radiology* **175**, 394-398.

Weissleder, R., Lee, A.S., Fischman, A.J., Reimer, P., Shen, T., Wilkinson, R., Callahan, R.J. & Brady, T.J. (1991). Polyclonal human immunoglobulin G labeled with polymeric iron oxide: antibody MR imaging. *Radiology* **181**, 245-249.

Weissleder, R., Lee, A.S., Khaw, B.A., Shen, T., & Brady, T.J. (1992). Antimyosinlabeled mono-crystalline iron oxide allows detection of myocardial infarct: MR antibody imaging. *Radiology* **182**, 381-385.

Weissleder, R. (2001). A clearer vision for in vivo imaging. Nature Biotechnology 2001, 19, 316-317.

Weissleder, R., Kelley, K., Sun, E.Y., Shtatland, T. & Josephson, L. (2005). Cell-specific targeting of nanoparticles by multivalent attachment of small molecules. *Nature Biotechnology* **23**, 1418-1423.

Wikipedia, the free encyclopedia: http://en.wikipedia.org/wiki/Quantum_dot.

Wikipedia, en.wikipedia.org/wiki/Computed_tomography.

Wikipedia, en.wikipedia.org/wiki/Single_photon_emission_computed_tomography.

Wikipedia, the free encyclopedia: en.wikipedia.org/wiki/Magnetic_resonance_imaging.

Wikipedia, the free encyclopedia, http://en.wikipedia.org/wiki/Medical_ultrasonography.

Wikipedia, the free encyclopedia, http://en.wikipedia.org/wiki/Positron_emission_tomography.

Willard, N.P. & Van Bommel, T. (2005). Ultrasound contrast agents for molecular imaging. *PCT/IB2005/053763*, Patent Filed on 15/11/2005.

Wilson, A.A., Ginovart, N., Hussey, D., Meyer, J. & Houle, S. (2002). In vitro and in vivo characterisation of [C-11]-DASB: a probe for in vivo measurements of the serotonin transporter by positron emission tomography. *Nuclear Medicine and Biology* **29(5)**, 509-515.

Winter, J.O., Liu, T.Y., Korgel, A, & Schmidt C.E. (2001). Recognition molecule directed interfacing between semiconductor quantum dots and nerve cells. *Advanced Materials* **13**, 1673-1677.

Winter, P.M., Neubauer, A.M., Caruthers, S.D., Harris, T.D., Robertson, J.D., Williams, T.A., Schmieder, A.H., Hu, G., Allen, J.S., Lacy, E.K., Zhang, H.Y., Wickline, S.A. & Lanza, G.M. (2006). Endothelial

alpha(v)beta3 integrin-targeted fumagillin nanoparticles inhibit angiogenesis in atherosclerosis. *Arteriosclerosis Thrombosis and Vascular Biology* **26**, 2103-2109.

Wisner, E.R., Katzberg, R.W., Koblik, P.D., McGahan, J.P., Griffey, S.M., Drake, C.M., Harnish, P.P., Vessey, A.R. & Haley, P.J. (1995). Indirect computed tomography lymphography of subdiaphragmatic lymph nodes using iodinated nanoparticles in normal dogs. *Academic Radiology* **2(5)**, 405-412.

Wisner, E.R., Weichert, J.P., Longino, M.A., Counsell, R.E. & Weisbrode, S.E. (2002). A surface-modified chylomicron remnant-like emulsion for percutaneous computed tomography lymphography - Synthesis and preliminary imaging findings. *Investigative Radiology* **37(4)**, 232-239.

Wolf, G.L., Shore, M.T., Bessin, G., McIntire, G.L., Bacon, E.R. & Illig, K.J. (1999). Lymph node extraction of radiopaque nanoparticulates in the rabbit as measured in vivo with CT. *Academic Radiology* **6**, 55-60.

Wu, E.X., Tang, H. & Jensen, J.H. (2004). Applications of ultrasmall superparamagnetic iron oxide contrast agents in the MR study of animal models. *NMR Biomedicine* **17**, 478-483.

Wu, X.Y., Li, H.J., Haley, K.N., Treadway, J.A., Larson, J.P., Ge, N.F., Peale, F. & Bruchez, M.P. (2003). Immunofluorescent labeling of cancer marker Her2 and other cellular targets with semiconductor quantum dots. *Nature Biotechnology* **21**, 41-46.

Xu, X. H. N., Brownlow, W. J., Kyriacou, S. V., Wan, Q., Viola, J. J. (2004). Real-time probing of membrane transport in living microbial cells using single nanoparticle optics and living cell imaging. *Biochemistry* **43**, 10400–10413.

Xu, R., Wang, Y., Wang, X., Jeong, E., Parker, D. L. & Lu, Z. (2007). In vivo evaluation of a PAMAM-Cystamine-(Gd-DO3A) conjugate as a biodegradable macromolecular MRI contrast agent. *Experimental Biology and Medicine* **232**, 1081-1089.

Yang, H., Santra, S., Walter, G.A. & Holloway, P.H. (2006). Gd-III-functionalized fluorescent quantum dots as multimodal imaging probes. *Advanced Materials* **18(21)**, 2890-+.

Young, I.R., Clarke, G.J., Bailes, D.R., Pennock, J.M., Doyle, F. H. & Bydder, G.M. (1981) Enhancement of relaxation rate with paramagnetic contrast agents in NMR imaging. *CT-Journal of Computed Tomography* **5 (6)**, 543-547.

Yu, S. & Watson, A.D. (1999). Metal-based X-ray contrast media. *Chemical Reviews* **99**, 2353-2377.

Yu, S.J., Kang, M.W., Chang, H.C., Chen, K.M. & Yu, Y.C. (2005). Bright fluorescent nanodiamonds: No photobleaching and low cytotoxicity. *Journal of the American Chemical Society* 127(50), 17604-17605.

Yuan, C., Mitsumori, L.M., Ferguson, M.S., Polissar, N.L., Echelard, D., Ortiz, G., Small, R., Davies, J.W., Kerwin, W.S. & Hatsukami, T.S. (2001). In vivo accuracy of multispectral magnetic resonance imaging for identifying lipid-rich necrotic cores and intraplaque hemorrhage in advanced human carotid plaques. *Circulation* **104**, 2051-2056.

Zhao, X., Hilliard, L.R., Mechery, S.J., Wang, Y.P., Bagwe, R.P., Jin, S.G. & Tan, W.H. (2004). A rapid bioassay for single bacterial cell quantitation using bioconjugated nanoparticles. *Proceedings of the National Academy of Sciences of the United States of America* **101**, 15027-15032.

Zheng, J.Z., Liu, J.B., Dunne, M., Jaffray, D.A. & Allen, C. (2007). In vivo performance of a liposomal vascular contrast agent for CT and MR-based image guidance applications. *Pharmaceutical Research* **24**, 1193-1201.

Zhu, Y., Peng, A.T., Carpenter, K., Maguire, J.A., Hosmane, N.S. & Takagaki, M. (2005). Substituted carborane-appended water-soluble single-wall carbon nanotubes: new approach to boron neutron capture therapy drug delivery. *Journal of American Chemical Society,* **127**, 9875-9880.

Zielhuis, S.W., Seppenwoolde, J.-H., Mateus,V.A.P., Bakker, C.J.G., Krijger, G.C., Storm, G., Zonnenberg, B.A., van het Schip, A.D., Koning, G.A. & Nijsen, J.F.W. (2006). Lanthanide-loaded liposomes for multimodality imaging and therapy. *Cancer Biotherapy & Radiopharmaceuticals* **21**, 520-527.

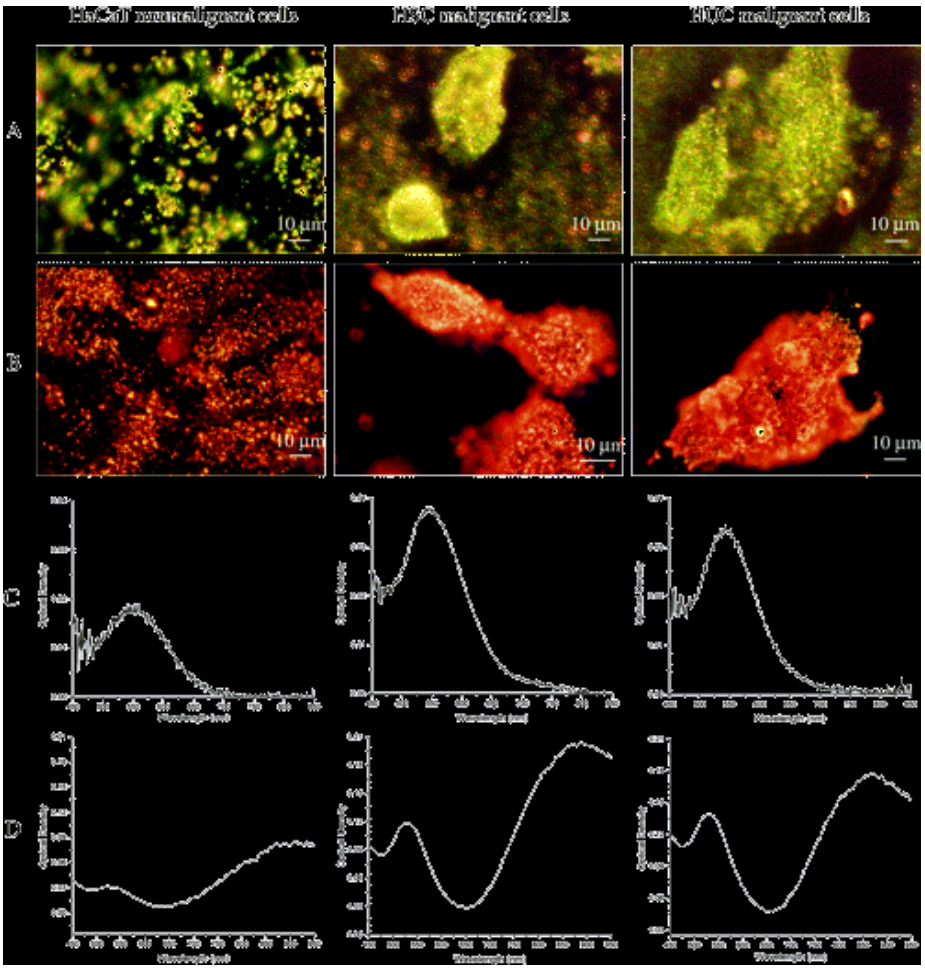

Figure 1. (A) Light scattering images of anti-EGFR/Au nanospheres after incubation with cells for 30 min at room temperature. (B) Light scattering images of anti-EGFR/Au nanorods after incubation with cells for 30 min at room temperature. (C) Average extinction spectra of anti-EGFR/Au nanospheres from 20 different single cells for each kind. (D) Average extinction spectra of anti-EGFR/Au nanorods from 20 different single cells for each kind. From gold nanospheres, the green to yellow color is most dominant, corresponding to the surface plasmonic enhancement of scattering light in the visible region, and from gold nanorods, the orange to red color is most dominant, corresponding to the surface plasmonic enhancement of the longitudinal oscillation in the near-infrared region (With permission adapted from Huang *et al.*, 2006b; Copyright © 2006 American Chemical Society).

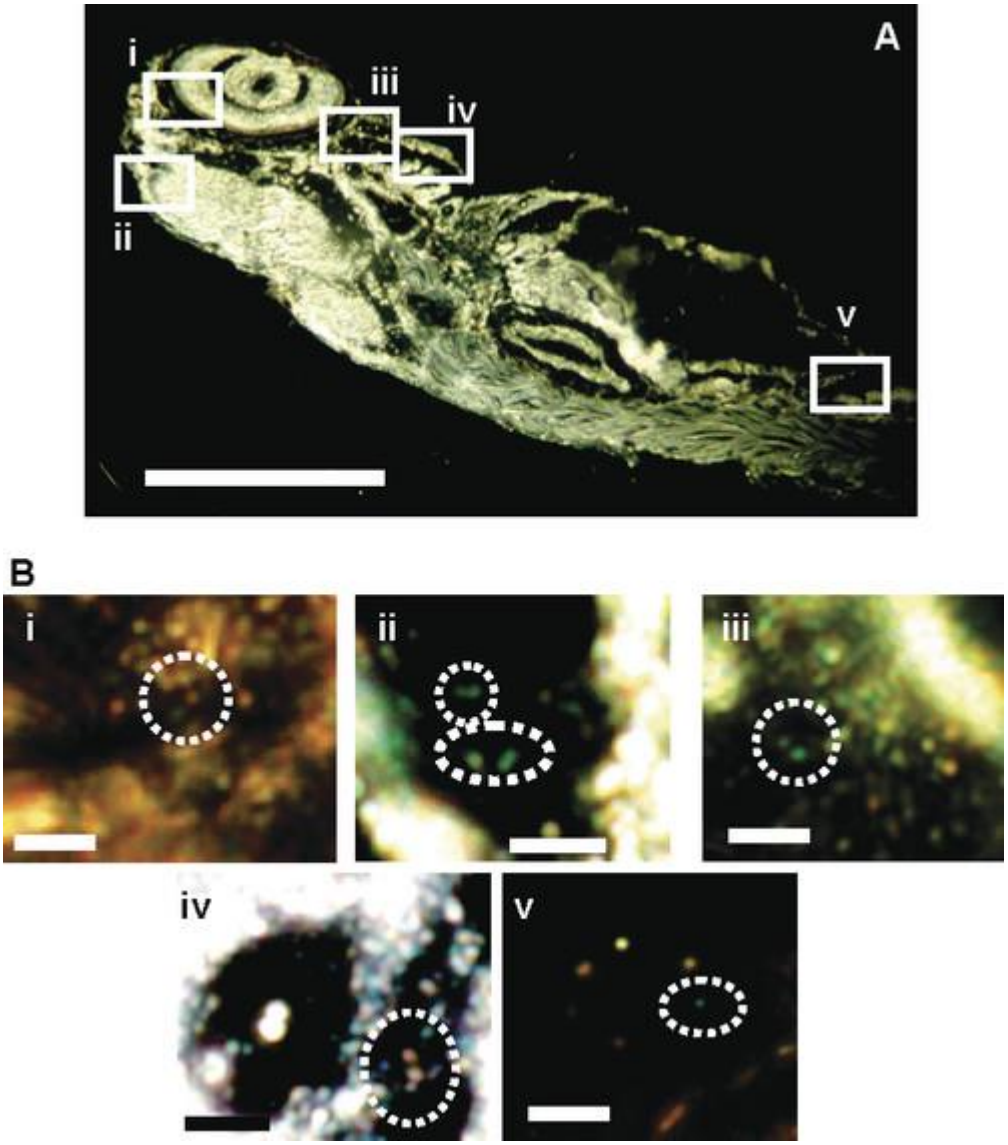

Figure 2. Characterization of individual Ag nanoparticles embedded inside a fully developed (120 hpf) zebrafish using dark-field SNOMS. (A) Optical image of a fixed, normally developed zebrafish. The rectangles highlight representative areas: (i) retina, (ii) brain (mesencephalon cavity), (iii) heart, (iv) gill arches, and (v) tail. (B) Zoom-in optical images of single Ag nanoparticles embedded in those tissue sections outlined in (A). Dashed circles outline the representative embedded individual Ag nanoparticles. Scale bar = 400 μm (A) and 4 μm (B) (With permission adapted from Lee *et al.*, 2007a; Copyright © 2007 American Chemical Society).

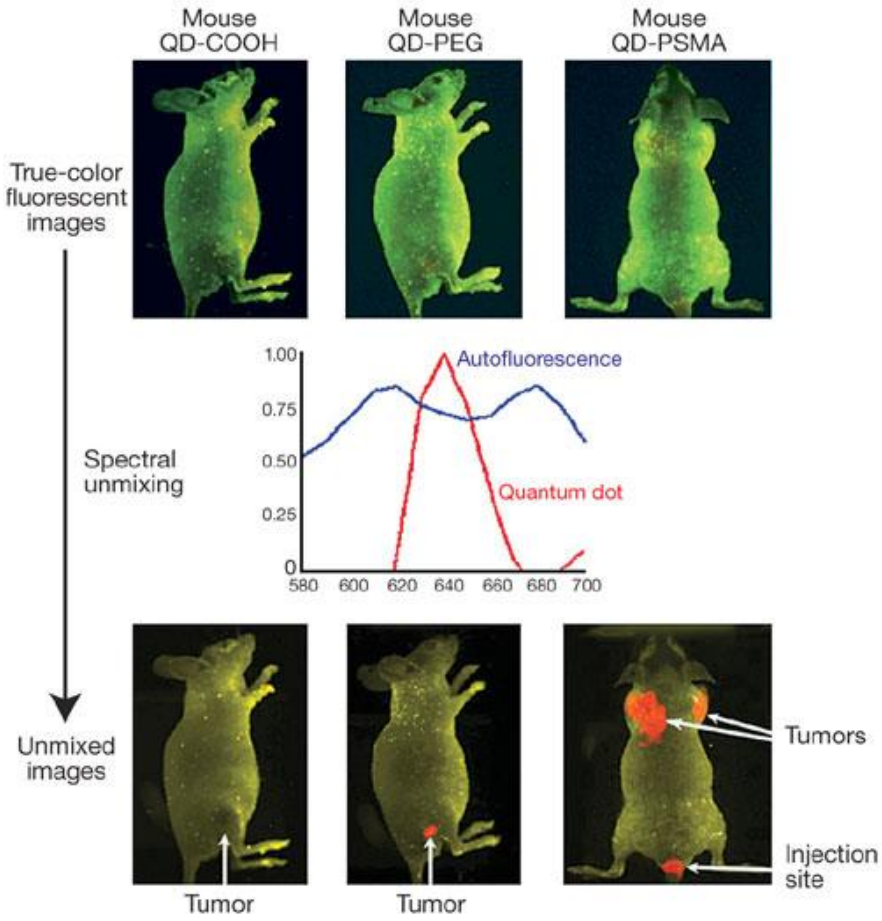

Figure 3. *In vivo* fluorescence images of tumor-bearing mice using QD probes with three different surface modifications: carboxylic acid groups (left), PEG groups (middle) and PEG-PSMA Ab conjugates (right). For each surface modification, a color image (top), two fluorescence spectra from QD and animal skin (middle) and a spectrally resolved image (bottom) were obtained from the live mouse models bearing C4-2 human prostate tumors of similar sizes (0.5−1.0 cm in diameter). The amounts of injected QDs and the lengths of circulation were: 6 nmol and 6 h for the COOH probe; 6 nmol and 24 h for the PEG probe; and 0.4 nmol and 2 h for the PSMA probe. The site of QD injection was observed as a red spot on the mouse tail. The spectral feature at 700 nm (red curve, middle panel) was an artifact caused by mathematical fitting of the original QD spectrum, which has little or no effect on background removal (With permission adapted from Gao *et al.*, 2004; Copyright © 2004 Nature Publishing Group).

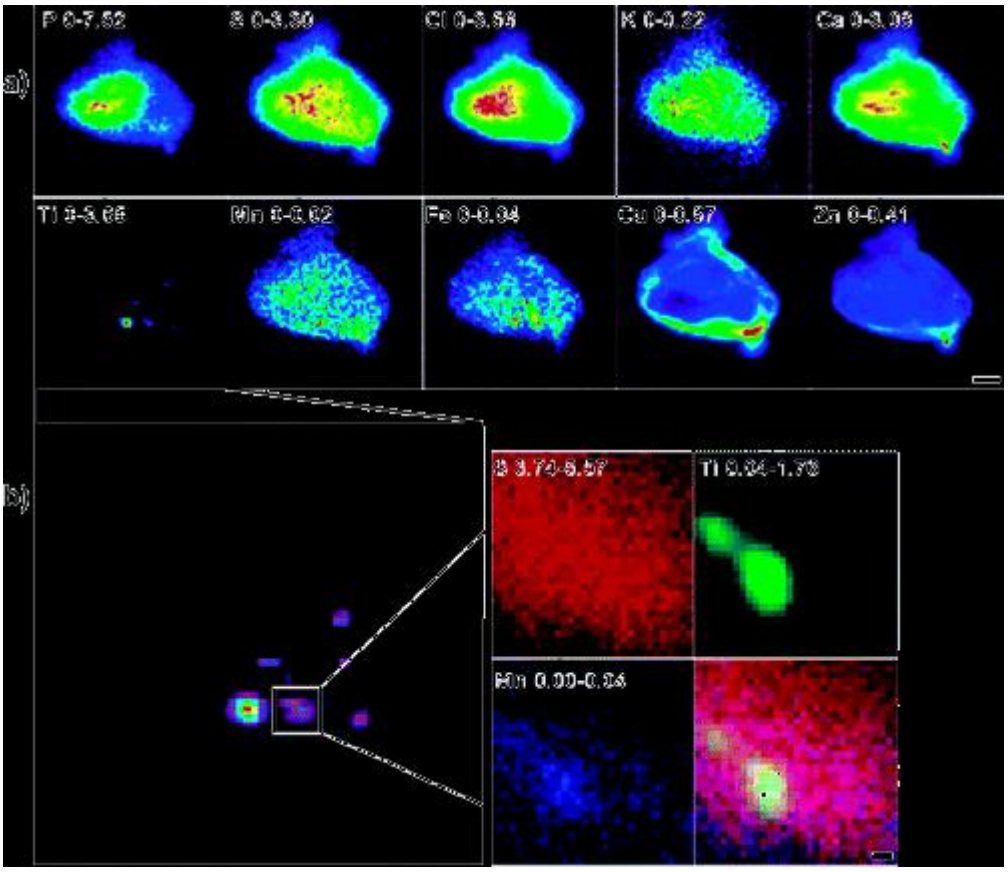

Figure 4. XFM maps of whole PC12 cell transfected with mitochondria-specific nanoconjugates using natural uptake. (a) Elemental maps of P, S, Cl, K, Ca, Ti, Mn, Fe, Cu, and Zn in PC12 cell treated with nanoconjugates carrying ND2s oligonucleotide for 24 h and then "washed" for 24 h in nanoconjugate-free medium. Elemental maps show the range of concentrations in the sample in a rainbow color scale from highest (red) to lowest (black) signal. Scan area was 13 μm × 12.8 μm, with 0.2 μm step. Scanning was done at 2ID-D beamline at the APS. Elemental concentrations are given in μg per cm^2. White size bar is 2 μm. (b) Enlarged Ti maps of the cells in (a) and a detailed XFM map of a mitochondria inside the cell. Left: enlarged Ti map of the whole cell. Right: S, Ti, Mn and overlap maps for the mitochondria-shaped form from the left panel. The scan area was 1.5 μm × 1.5 μm with 50 nm step. Scanning was done at 2ID-D beamline at the APS. White size bar is 100 nm (With permission adapted from Paunesku *et al.*, 2007; Copyright © 2007 American Chemical Society).

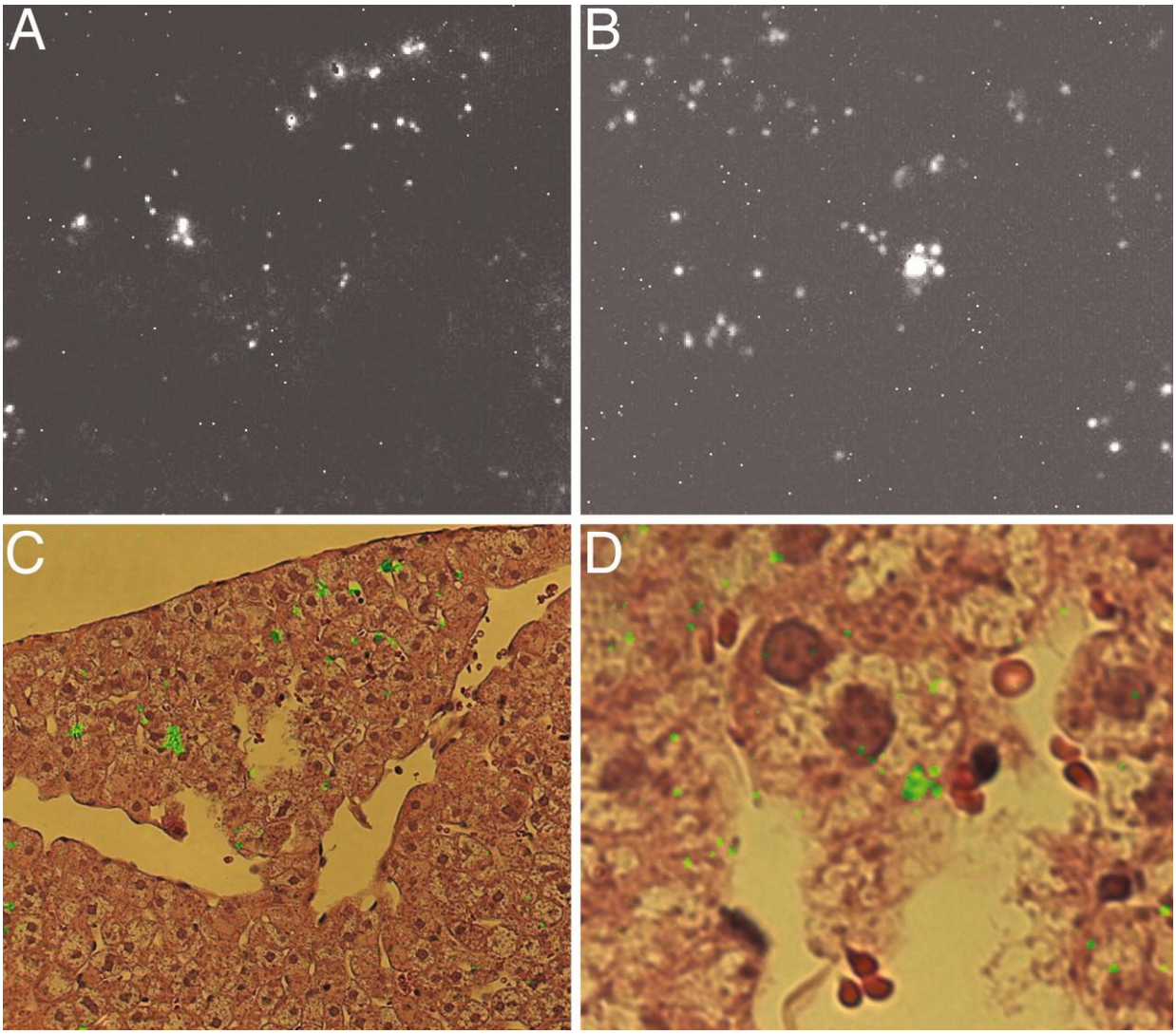

Figure 5. Micrographs at two magnifications of liver tissue from rabbits killed 24 h after i.v. administration of suspended SWNTs. (*A* and *B*) Near-IR SWNT fluorescence images with field widths of 390 µm (*A*) and 83 µm (*B*). Scattered isolated bright pixels are artifacts from defective sensor elements in the near-IR camera; all larger features represent emission from SWNTs. In *C* and *D*, the SWNT fluorescence from *A* and *B* is shown overlaid as false-color green onto visible bright-field images from adjacent 3-µm-thick specimen slices that had been stained with hematoxylin and eosin (With permission adapted from Cherukuri *et al.*, 2006, Copyright © 2006 by the National Academy of Sciences).

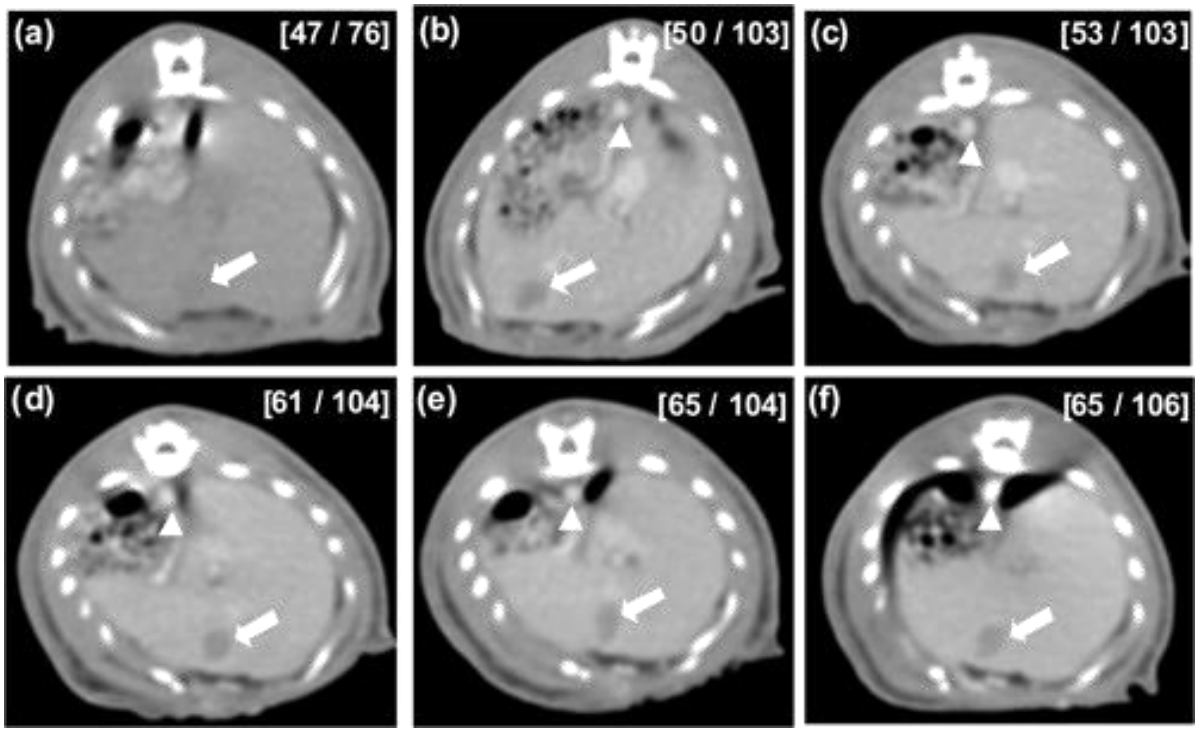

Figure 6. Serial CT images in a rat hepatoma model following injection of 400 μL of PEG-coated GNPs (100 mg/mL) into the tail vein. Images were obtained at (a) 0 h (before injection) and (b) 5 min, (c) 1 h, (d) 2 h, (e) 4 h, and (f) 12 h after injection. Arrows indicate the hepatoma regions, and the arrowheads indicate the aorta. Numbers in brackets are the HU values of the hepatoma regions (left) and the surrounding normal liver parenchyma (right) (With permission adapted from Kim *et al.*, 2007, Copyright © 2007 by American Chemical Society).

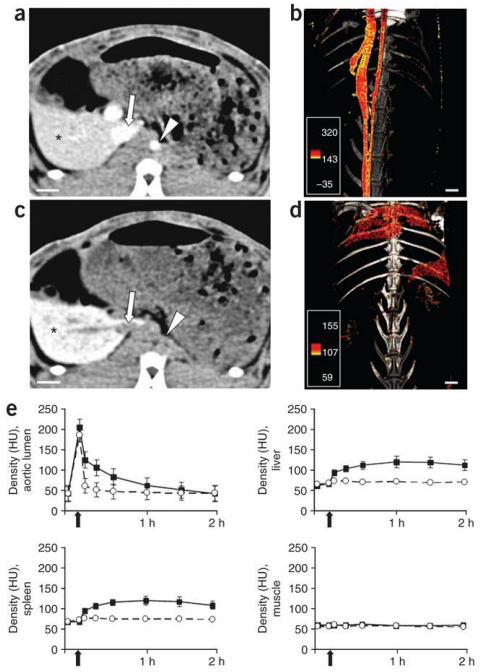

Figure 7. Kinetics and distribution of N1177 in nonatherosclerotic rabbits. (**a,b**) Axial view (acquired by CT) of a nonatherosclerotic rabbit 5 min after the injection of N1177 (**a**) showing the enhancement of the aorta (white arrowhead) and vena cava (white arrow), allowing for the reconstruction of three-dimensional CT angiograms (**b**). (**c**) Two hours after the injection of N1177, a strong enhancement was detected in the spleen (asterisk), as shown in the axial CT view of the rabbit. (**d**) The regions of high densities were identified on a three-dimensional reconstruction of the CT scan using a color scale. Note the strong enhancement of the spleen and the liver 2 h after the injection of N1177. The same level and width windows were used for images **a** and **c**. Inserts in **b** and **d** indicate the color scale of densities in HU. (**e**) Densities in HU of the different organs (assessed by CT) before and at different time points after the injection of N1177 (squares) or a conventional iodinated contrast agent (circles). Densities measured in macrophage-rich organs were significantly higher 2 h after the injection of N1177 compared to precontrast values, whereas no enhancement was detected in these organs 2 h after the injection of a conventional CT contrast agent. Black arrows denote the time of injection (With permission adapted from Hyafil *et al.*, 2007; Copyright © 2007 Nature Publishing Group).

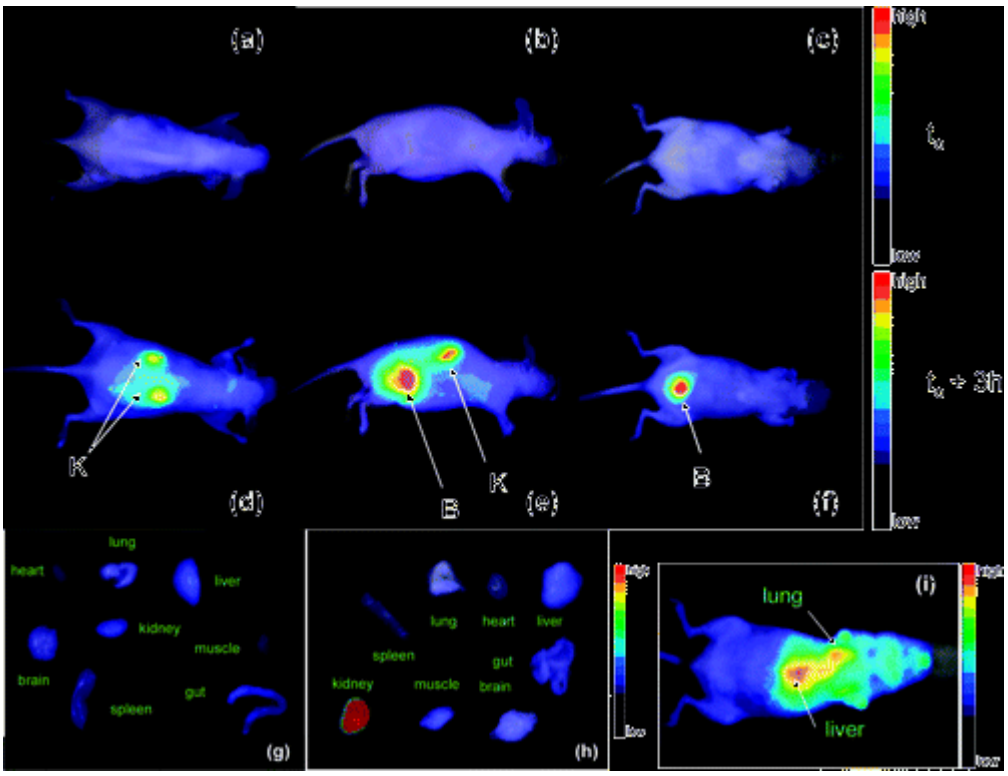

Figure 8. Fluorescence reflectance imaging of a nude mouse (a, b, c) before and (d, e, f) 3 hours after the injection of GadoSiPEG2C (K, kidneys; B, bladder). Fluorescence reflectance imaging of some organs after dissection (g) of a control mouse (no particles injection) and (h) of the nude mouse visualized on pictures (a-f). (i) Fluorescence reflectance imaging of a nude mouse after the injection of GadoSi2C (particles without PEG). Each image is acquired with an exposure time of 200 ms (With permission adapted from Bridot *et al.*, 2007; Copyright © 2007 American Chemical Society).

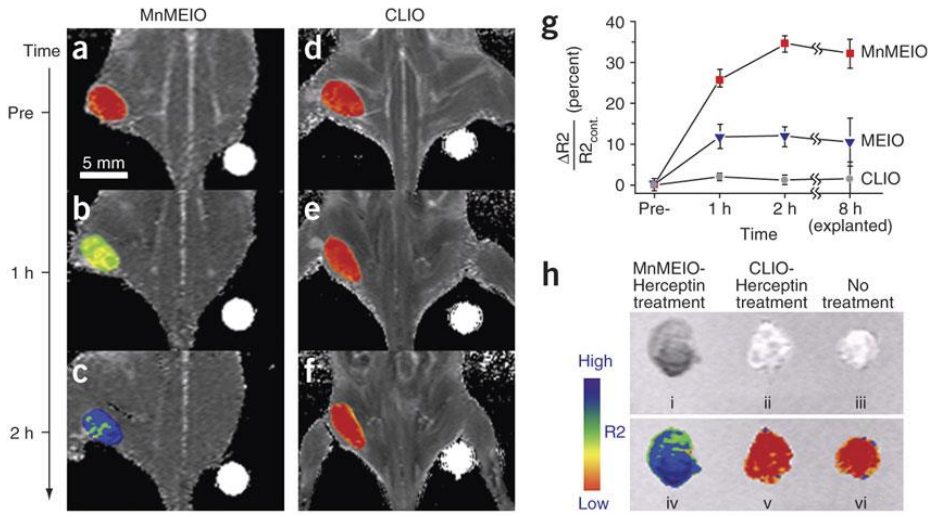

Figure 9. In vivo MR detection of cancer using magnetic nanoparticle–Herceptin conjugates. (a–f) Color maps of T2-weighted MR images of a mouse implanted with the cancer cell line NIH3T6.7, at different time points after injection of MnMEIO-Herceptin conjugates or CLIO-Herceptin conjugates (preinjection (a,d); and 1 h (b,e) or 2 h (c,f) after injection). In a–c, gradual color changes at the tumor site, from red (that is, low R2) to blue (that is, high R2), indicate progressive targeting by MnMEIO-Herceptin conjugates. In contrast, almost no change was seen in the mouse treated with CLIO-Herceptin conjugate (d–f). (g) Plot of R2 change versus time. In the mouse treated with MnMEIO-Herceptin conjugate (squares), significant R2 changes (up to 34%) were observed with time after treatment. In contrast, R2 changed by <5% after treatment with CLIO-Herceptin conjugate (dots) and by <13% after treatment with 12-nm-MEIO–Herceptin conjugate (triangles). (h) Ex vivo MR images (i–iii) of explanted tumors (8 h) and their color maps (iv–vi). Tumor explanted after treatment with MnMEIO-Herceptin conjugate (i) is dark; that explanted following CLIO-Herceptin conjugate treatment (ii) or no treatment (iii) shows no contrast. Consistently, in the image color-coded according to R2, the tumor explanted after MnMEIO-Herceptin conjugate treatment is blue (iv) whereas that after CLIO-Herceptin conjugate treatment (v) or no treatment (vi) is red (With permission adapted from Lee *et al.*, 2007c; Copyright © 2007 Nature Publishing Group).

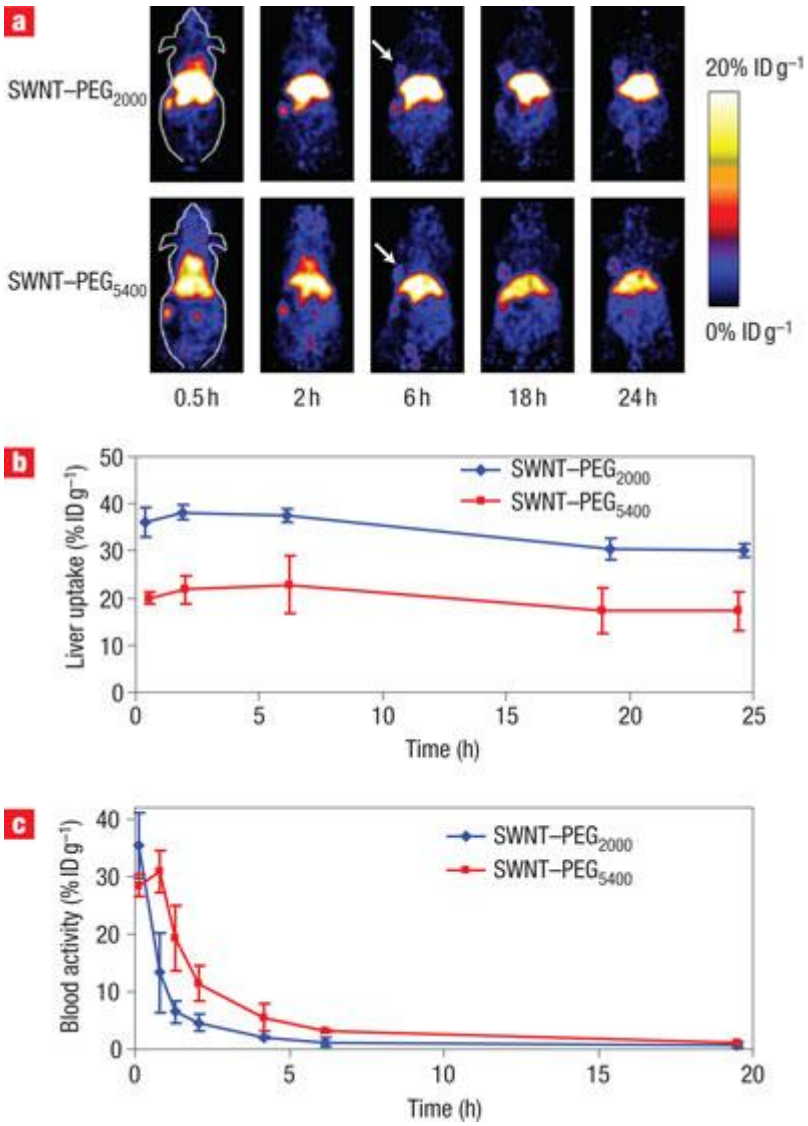

Figure 10. Functionalization-dependent biodistribution and blood circulation of intravenously injected SWNTs in mice bearing the U87MG human glioblastoma tumour. a, MicroPET images of two mice at various time points post tail-vein injection of 64Cu-labelled SWNT–PEG2000 and SWNT–PEG5400, respectively. The arrows point to the tumours. b, Liver uptake curves over time as measured by PET for the two SWNT conjugates. c, Blood activity curves for the two conjugates. All data points represent three animals per group (four mice per group for c) (With permission adapted from Liu *et al.*, 2007b; Copyright © 2007 Nature Publishing Group).

	Molec. Info.	Func. Info.	Anat. Info.	Reslolution (mm)	Depth (cm)	Contrast Conce.	Cost	Comments
CT/ SPECT	+++	++	+	1-2	No Limit	pM-nM	++	Very sensitive, Range of nuclides and energies, Anat. Info.
PET	+++	++	+	1-2	No Limit	<pM-nM	+++	Very sensitive, Quantitation
MR	++	+++	+++	0.01-0.1	No Limit	mM-μM	+++	No radiation, smart contrast agents, Molec. Func., Anat. Info.
OI	+++	++	+	Limit, Depth-dependent	<8	nM	+	No radiation, Small devices, Multi-Wavelength Imaging, Smart contrast agents
USG	++	+++	+	<0.0001-1.1(Axial) 1.0-2.8 (Lateral) with frequency dependent	Frequency-dependent	pM-nM	+	No radiation, smart contrast agents, Molec. Func., Anat. Info.

Table 1: Comparison of various biological and medical imaging modalities (Adapted partly from Hengerer et al., 2005; Elliott & Thrush, 1996; Ferrara, Pollard & Borden, 2007).

CT: Computed Tomography; SPECT: Single-Phonton Emission Computed Tomography; PET: Poistron Emission Tomography; MRI: Magnetic Resonance Imaging; OI: Optical Imaging; USG: Ultrasonography; Molec. Info.: Molecular Information; Anat. Info.: Anatomy Information; Contrast Conc.: Contrast Concentration

Contrast media	magnetic components	Size	Tested for humans?	MR applications	Comments
Albumin-(Gd-DTPA)30	Gd	92 kDa	No	Tumor angiogenesis, Angiography, Mammography	Experimental only. Also used in anti-angiogenesis drug research
MS-325	Gd	68 kDa	Yes	Angiography, Lymphangiography	
Dextran-(Gd-DTPA)15	Gd	75 kDa	Yes	Angiography, Cardiac perfusion studies	High polydispersity. Also used to coat liposomes and iron oxide MMCMs
Dextran-(Gd-DTPA)187	Gd	165 kDa	Yes	Blood pool	High vascular residence time
Liposomes	Gd or Iron	20–400 nm	No	Liver and spleen imaging, Lymhangiography	High polydispersity. Good potential for drug delivery
Viral particles: CCMV	Gd	28 nm	No	Angiogenesis	Developmental stages only
Dendrimers	Gd	15 kDa (G2), 88 kDa (G5), 3820 kDa (G10)	No	Lymphangiography, Tumor vasculature (larger generations)	Potential for targeting imaging and drug delivery
SPIO	Iron	50–150 nm	Yes	Liver metastases	Negative contrast agents. Ferumoxides licensed for liver imaging
USPIO	Iron	10–50 nm	Yes	Lymphangiography, Tumor angiogenesis	Potential for drug delivery, targeted imaging and stem cell imaging
VSOP	Iron	2–10 nm	No	Angiography	

Table 2: Comparison of some contrast media for MRI applications (Adapted partly from Barrett *et al.*, 2006). MMCM: Macromolecular contrast media, Gd: Gadolinium, kDa: kilo-Daltons, nm: nanometers, CCMV: cowpea chlorotic mottle virus, SPIO: superparamagnetic iron oxide, USPIO: ultrasmall superparamagnetic iron oxide, VSOP: very small superparamagnetic iron oxide.